מכון ויצמן למדע
WEIZMANN INSTITUTE OF SCIENCE

Dynamics of social representation in the mouse prefrontal cortex

Document Version:
Accepted author manuscript (peer-reviewed)

Citation for published version:
Levy, DR, Tamir, T, Kaufman, M, Parabucki, A, Weissbrod, A, Schneidman, E & Yizhar, O 2019, 'Dynamics of social representation in the mouse prefrontal cortex', *Nature Neuroscience*, vol. 22, no. 12, pp. 2013-2022. https://doi.org/10.1038/s41593-019-0531-z

Total number of authors:
7

Digital Object Identifier (DOI):
10.1038/s41593-019-0531-z

Published In:
Nature Neuroscience

License:
Unspecified

General rights
@ 2020 This manuscript version is made available under the above license via The Weizmann Institute of Science Open Access Collection is retained by the author(s) and / or other copyright owners and it is a condition of accessing these publications that users recognize and abide by the legal requirements associated with these rights.

How does open access to this work benefit you?
Let us know @ library@weizmann.ac.il

Take down policy
The Weizmann Institute of Science has made every reasonable effort to ensure that Weizmann Institute of Science content complies with copyright restrictions. If you believe that the public display of this file breaches copyright please contact library@weizmann.ac.il providing details, and we will remove access to the work immediately and investigate your claim.

(article begins on next page)

Dynamics of social representation in the mouse prefrontal cortex

Dana Rubi Levy[1]*, Tal Tamir[1]*, Maya Kaufman[1], Ana Parabucki[1], Aharon Weissbrod[1], Elad Schneidman[1] and Ofer Yizhar[1]

[1]*Department of Neurobiology, Weizmann Institute of Science, Rehovot, Israel.*

* These authors contributed equally to this manuscript: Dana Rubi Levy, Tal Tamir.

Correspondence to: ofer.yizhar@weizmann.ac.il

Abstract

The prefrontal cortex (PFC) plays an important role in regulating social functions in mammals, and its dysfunction has been linked to social deficits in neurodevelopmental disorders. Yet little is known of how the PFC encodes social information and how social representations may be altered in such disorders. Here, we show that neurons in the medial PFC of freely behaving male mice preferentially respond to socially relevant olfactory cues. Population activity patterns in this region differed between social and nonsocial stimuli and underwent experience-dependent refinement. In mice lacking the autism-associated gene *Cntnap2*, both the categorization of sensory stimuli and the refinement of social representations were impaired. Noise levels in spontaneous population activity were higher in *Cntnap2* knockouts and correlated with the degree to which social representations were disrupted. Our findings elucidate the encoding of social sensory cues in the medial PFC and provide a link between altered prefrontal dynamics and autism-associated social dysfunction.

Introduction

Social interactions are a central aspect of animal behavior and are orchestrated by multiple neural circuits throughout the brain. The complexity of social behaviors requires the constant integration of sensory cues with internal motivational and arousal states, as well as the coordination of intricate motor sequences[1,2]. The PFC is known to integrate such internal and external variables3 and is crucial for social functions in humans[4,5] and other animals[6–9]. Neurons in the PFC represent multiple aspects of the external world, responding to salient sensory cues associated with positive or negative reinforcement and display mixed selectivity toward combinations of task-related variables[10,11]. In social contexts, neural activity in the PFC increases during approach toward a conspecific[9] and represents both spatial and social aspects of behavior[8]. Yet little is known regarding the response selectivity of PFC neurons to social sensory cues, and the dynamics of social representations in prefrontal circuits remain largely unexplored.

Impairments of the PFC have been widely reported in autism spectrum disorder (ASD)[12–14], a neurodevelopmental disorder associated with altered social function. Although the pathophysiology of autism is not well understood, a leading theory suggests that ASD arises from developmental changes in the balance of neo- cortical excitation and inhibition (E/I balance)[15]. This functional imbalance is hypothesized to disrupt the maturation of cortical synaptic connections[16,17], leading to changes in information processing and elevated cortical noise[18]. Accordingly, imaging studies have identified reduced long-range prefrontal connectivity in humans with autism-associated gene variants[19], and demonstrated poor selectivity to sensory stimuli20 and higher trial-to-trial variability in humans with ASD[21]. Although some studies using animal models of the disorder have reported similar findings, most of our knowledge regarding autism-associated changes in the functional properties of cortical neurons is based on ex vivo studies, and very little is known about the emergent changes in circuit function and dynamics in behaving animals[17].

Here, we studied the representation of social information in the medial PFC (mPFC) of freely behaving mice. To characterize the nature of neural coding and stimulus processing in social dysfunction, we compared neural activity in wild-type (WT) mice and *Cntnap2* knockout (*Cntnap2*$^{-/-}$) mice, an established genetic model of autism[22]. We found that in WT mice, mPFC neurons displayed robust response selectivity to social compared with nonsocial sensory cues. Population-level analysis revealed distinct categorization of sensory cues based on their social nature, which

underwent marked experience-dependent refinement over experimental sessions. In *Cntnap2*$^{-/-}$ mice, mPFC activity showed reduced differentiation between social and nonsocial stimuli and lacked experience-dependent dynamics. Strikingly, the deficits in social-specific activity patterns in *Cntnap2*$^{-/-}$ mice were strongly correlated with elevated variability of spontaneous neuronal activity. Our results uncover distinct coding of social sensory cues in the mPFC and provide a potential link between ongoing cortical dynamics, encoding of socially relevant stimuli and autism-associated social dysfunction.

Results

mPFC neurons are tuned to social cues

Social behaviors in rodents are primarily guided by the emission and detection of specific chemosensory cues[1,23]. To study the responses of prefrontal neurons to social cues, we used a custom-built odor delivery system, which enabled the precise presentation of olfactory stimuli while recording mPFC activity in freely behaving male mice (Fig. 1a,b; Extended Data Fig. 1a,b). Each mouse was repeatedly presented (in a pseudorandomized order) with the odors of male mice and female mice and with the following three nonsocial odors of distinct valence: banana oil, considered to be a neutral stimulus to mice[24]; peanut butter oil, an attractive stimulus[24]; and hexanal, known to be mildly repellent[25]. In interleaved control trials, clean air was presented using the same odor delivery system. Mice displayed pronounced behavioral responses following presentation of the odors, which consisted of orienting toward the odor port and increased locomotion. The probability of odor-directed orientation responses was higher during the delivery of social cues (Fig. 1c). However, the response latency (Fig. 1d) and the stimulus-evoked increase in locomotion (Fig. 1e) did not significantly differ between social and nonsocial stimuli.

We recorded stimulus-evoked responses of mPFC units (n = 194; 6 mice) and found that 44% responded to at least one stimulus, typically by increasing their firing rates (FRs; Fig. 2a-c; Extended Data Fig. 2a–c). Presentation of both male and female cues recruited more mPFC units than any of the nonsocial odors (Fig. 2b). Almost one- quarter of the recorded units displayed selectivity to social signals; a value that was twice the number of units with nonsocial odor selectivity or mixed social/nonsocial responses (Fig. 2c, left; Extended Data Fig. 2c–e). In addition, the magnitude of neuronal responses to social odors was significantly higher (Fig.

2b,d; Extended Data Fig. 2f). Among responsive units, 51% were stimulus-specific, of which a large fraction responded exclusively to male or female cues (Fig. 2c, right). The average unit tuning, calculated as the normalized odor-evoked response magnitude in all units that showed stimulus-associated responses, was higher for both male and female cues than for all nonsocial odors, regardless of odor identity (Fig. 2e). This social preference in unit tuning was independent of stimulus concentration (Extended Data Fig. 3a,b).

Distinct population representations of social and nonsocial stimuli in the mPFC

To further elucidate the nature of prefrontal representation of social signals, we analyzed the activity patterns of simultaneously recorded mPFC neurons (14–23 units per mouse; Fig. 3a). First, we discretized neural responses into 150-ms bins and then used principal component analysis (PCA) to project the population FRs as a function of time onto the first two principal components (PCs; see Methods). This analysis revealed a clear divergence of population responses evoked by the social and nonsocial stimuli soon after stimulus onset (Fig. 3b, middle; Supplementary Video 1). This category-specific separation of population trajectories persisted for several seconds after stimulus offset before converging back to baseline activity state (Fig. 3b, right).

To quantify these differences and to explore the detailed structure of the population code, we discretized neural responses of 30 randomly selected groups of 10 cells from each mouse into 20-ms bins and fitted maximum entropy models to the distributions of population activity patterns evoked by each of the presented stimuli (for each group of cells, we fit both a first-order and a second-order model, and used the one that gave higher cross-validation values; see Extended Data Fig. 4)[26,27]. We quantified the dissimilarity between the distributions of stimulus-evoked population responses (encoding distributions) using the Jensen–Shannon divergence method, $d(si,sj)$= Djs[p(r|si)||p(r|sj)], which measures in bits their distinguishability (d = 0 would indicate indistinguishable distributions, while d = 1 indicates completely nonoverlapping responses; Fig. 3a, lower, see Methods)[28]. We calculated the dissimilarity between all pairs of encoding distributions and averaged these distances across mice (presented in bits s^{-1} to give the rate of information about representation similarity; Fig. 3c). The block-diagonal structure of the dissimilarity matrix reflects a category-based organization of the population codebook in the mPFC. The encoding distributions of the social cues were significantly more similar to each other than to any of the nonsocial odors, regardless of odor identity or valence (Fig. 3d), and independent of odor stimulus concentration (Extended Data Fig. 3c,d). We further explored the

divergence of stimulus encoding over time and found that while population activity patterns were indistinguishable during the baseline period, representations of social and nonsocial signals diverged within 2 s following stimulus onset and slowly returned to baseline levels after stimulus offset (Fig. 3e).

Altered representation of social stimuli in the mPFC of *Cntnap2*$^{-/-}$ mouse model of autism

Having observed distinct representations of social cues in the mPFC population code, we tested whether the mPFC representation of social signals is disrupted in animals that display impaired social function, such as those observed in ASD. In humans, mutations in the *CNTNAP2* (also known as *CASPR2*) gene are strongly associated with ASD risk[29], and patients that carry risk-associated variants of this gene show altered prefrontal connectivity[19]. Mice lacking the *Cntnap2* gene present all of the core behavioral phenotypes of autism and several associated neuronal phenotypes[22]. We therefore presented *Cntnap2*$^{-/-}$ mice with the same set of social and nonsocial stimuli, using their age-matched wild-type littermates as controls (*Cntnap2*$^{+/+}$; referred to as WT hereafter; $n_{Cntnap2\text{-}/\text{-}} = 6$, $n_{WT} = 5$). To characterize how population representations in the mPFC might undergo experience-dependent refinement, we compared stimulus-evoked neuronal responses in two consecutive recording sessions conducted in each mouse less than 1 week apart. In contrast to the previous experiment described in Figs. 1–3, in which mice were exposed to the odors before recording sessions, mice in the current experiment were habituated to the chamber but were not previously presented with the odor repertoire.

To confirm previous reports of social deficits in *Cntnap2*$^{-/-}$ mice, we conducted a battery of behavioral tests comparing knockout mice to WT littermates. We found that WT mice showed robust social preference in the three-chamber social test (Fig. 4a,b) and a preference for exploration of social odors in an odor-approach assay utilizing the same odor repertoire and delivery apparatus described above (Fig. 4c,d). In contrast, *Cntnap2*$^{-/-}$ mice did not present any preference toward social stimuli in the three-chamber test, and showed reduced preference toward social odors in the odor- approach assay (Fig. 4a–d). However, in the olfactory-guided buried food-finding test, *Cntnap2*$^{-/-}$ mice performed indistinguishably from their WT littermates (Extended Data Fig. 5c), which is consistent with previous reports of intact olfactory function in these mutants[22]. To more directly explore the detection of the olfactory cues presented in this study, we used the odor-infusion system to record sniffing signals from freely moving *Cntnap2*$^{-/-}$ mice and WT controls (Fig. 4e–g). In both genotypes, we observed a significant increase in the

frequency of sniffs in response to the presentation of odor stimuli compared to clean air. Importantly, sniffing responses of *Cntnap2*$^{-/-}$ mice to all odors were indistinguishable from those of WT mice, which suggests that olfactory investigation of the presented odors was intact (Fig. 4f,g).

We recorded a total of 269 units in *Cntnap2*$^{-/-}$ mice (133 on day 1 and 136 on day 2) and 237 in WT littermates (125 on day 1 and 112 on day 2; Extended Data Fig. 6). We found that while WT mice maintained a preference in unit response profile to social cues, this bias was lost in *Cntnap2*$^{-/-}$ mice (Fig. 5a,b). The distribution of unit selectivity shifted significantly between the two recording sessions in WT mice. That is, the number of mixed-response units decreased between experimental sessions, whereas the percentage of units specifically responding to social or nonsocial stimuli, and the percentage of cue-specific units, increased (Fig. 5a; Extended Data Fig. 7). *Cntnap2*$^{-/-}$ mice showed a similar decrease in the percentage of mixed-response units, but this was accompanied by an increase in the percentage of nonresponsive units (from 44% on day 1 to 58% on day 2; Fig. 5a). The normalized magnitude of neuronal responses to social cues was significantly larger than for all nonsocial odors in WT mice, whereas this difference was significantly attenuated in *Cntnap2*$^{-/-}$ mice (Fig. 5b). Importantly, the magnitude of stimulus-evoked neuronal responses was not correlated with behavioral loco- motion in any of the genotypes or stimuli (Supplementary Table 1). The behavioral responses of the recorded mice during 5 s of odor presentation were also similar between genotypes, which is consistent with our previous findings of intact olfactory function in *Cntnap2* mutants (Extended Data Fig. 5e,f).

To examine the population activity in WT and *Cntnap2*$^{-/-}$ mice, we again projected the stimulus-evoked population FRs onto the first two PCs (as in Fig. 3b). Differences between WT and *Cntnap2*$^{-/-}$ mice in population responses to the odors were clearly apparent in this low-dimensional embedding. That is, while WT trajectories prominently diverged in the PC space based on social category (similar to the data acquired in the original cohort shown in Fig. 3), *Cntnap2*$^{-/-}$ trajectories did not show clear category-level separation (Fig. 5c; Supplementary Videos 2 and 3).

Social representations undergo experience-dependent refinement in WT but not in *Cntnap2*$^{-/-}$ mice

In patients with ASD, a disruption in plasticity-related processes has been proposed as an endophenotype of the disorder[30,31]. Consistent with these findings, several animal models of ASD display impairments in long-term synaptic plasticity[32]. We therefore measured the experience-dependent changes in mPFC population representations of odor stimuli by performing two

recording sessions in each mouse, separated by 2–5 days. Again, we fitted a maximum entropy model to the population activity of 30 randomly selected groups of 10 cells in each mouse to each of the stimuli for each of the 2 days, and then compared the stimulus-evoked encoding distributions. While mPFC encoding in WT mice showed distinct social and nonsocial separation already in the first recording session, the distance between responses to odors from the two categories grew significantly larger on the second session (Fig. 5d, upper), demonstrating a significant effect of experience. In contrast, the separation between the representations of social and nonsocial cues in *Cntnap2*$^{-/-}$ mice was both less pronounced on the first session compared with WT mice and did not improve on the following one (Fig. 5d, lower).

To quantify the separation between representation of social (S) and nonsocial (NS) stimuli for each mouse, we calculated a social distinction index, SDI=$\ln\left(\frac{d(S;NS)}{d(S;S)}\right)$, where *d*(S;NS) denotes the average distance between social and nonsocial stimuli and *d*(S;S) is the distance between social stimuli. The SDI values consistently and significantly increased between the first and second recording days for all WT mice, which indicated an increased divergence between stimulus categories. In contrast, no consistent change occurred in the *Cntnap2*$^{-/-}$ group, and mean SDI values in these mice remained unchanged between sessions (Fig. 5e). We further found that in WT mice, the encoding distances within each category (d(S;S) and d(NS;NS)) decreased between recording sessions, while the inter-category distance d(S;NS) increased. In *Cntnap2*$^{-/-}$ mice, however, no significant change occurred in either of these distances (Fig. 5f).

Decoding of stimulus identity and category from mPFC population activity

To evaluate mPFC encoding of odor identity at the level of single trials, we used a maximum likelihood classifier based on the encoding models of the stimulus-evoked population activity. Models were trained on seven out of eight presentations of each stimulus and used to estimate the likelihood of odor identity for each one of the held-out test trials (all possible combinations of seven train trials and one test trial were calculated for each stimulus, see Methods). In all mice, we could reliably decode both social and nonsocial odors from single-trial population activity. Averaged likelihood values in WT mice were similar for cues of the same category, but lower for odors of the other category. Conversely, likelihood values in *Cntnap2*$^{-/-}$ mice were similar for all odors regardless of social category (Fig. 6a,b).

We evaluated the performance of the decoders by the probability that the model of each stimulus would have the maximal likelihood value, given the presentation of a specific odor (Fig.

6c). Performance was well above chance for the correct odor in both WT and *Cntnap2*$^{-/-}$ mice. However, while rare in WT mice, decoding errors between categories were common in *Cntnap2*$^{-/-}$ mice. Furthermore, the decoding results in WT mice demonstrated increased error rates within the nonsocial category (represented by the overlapping areas in Fig. 6c), which suggests that there is a generalization of the representation of nonsocial odors. To directly quantify the difference between genotypes, we next trained a stimulus-category decoder for social versus nonsocial odors and compared the results to those of the stimulus-identity decoder. Remarkably, the decoding performance for individual odors was similar in WT and *Cntnap2*$^{-/-}$ mice, whereas the performance for odor category (S or NS) was significantly inferior in *Cntnap2*$^{-/-}$ mice (Fig. 6d). These findings suggest that *Cntnap2*$^{-/-}$ mice have specific deficits in odor categorization, rather than in the encoding of stimulus identity.

Increased neuronal noise in mPFC activity of *Cntnap2*$^{-/-}$ mice correlates with altered social representations

We then tested what features of single cell or population activity might underlie the differences in the mPFC representation of social and non-social cues in WT and *Cntnap2*$^{-/-}$ mice. Previous studies have demonstrated altered synaptic properties[16] and decreased long-range connectivity patterns[33] in the mPFC of *Cntnap2*$^{-/-}$ mice, findings that might reflect homeostatic adaptations to an altered excitation-inhibition balance in ASD[15,34,35]. The cortical E/I balance has been suggested to affect neuronal FR and correlations[18,36], noise at the level of single cells[37], and signal and noise correlations in the network[18]. We therefore compared these features of mPFC cell and network activity patterns between WT and *Cntnap2*$^{-/-}$ mice. We specifically focused on baseline activity, before stimulus onset, as it characterizes the properties of the network regardless of stimulus presentation.

The differences between WT mice and *Cntnap2*$^{-/-}$ mice were already apparent by projecting the baseline activity patterns onto the first two PCs of population activity, as shown in Fig. 7a (and in Supplementary Videos 2 and 3). In WT mice, baseline trajectories were separated from stimulus-evoked trajectories (but overlapped with the clean air trajectory), whereas all trajectories overlapped in *Cntnap2*$^{-/-}$ mice. We further found that the baseline FRs of mPFC units in *Cntnap2*$^{-/-}$ mice were significantly higher than those recorded in their WT littermates, whereas the pairwise correlations between units recorded in knockout mice were lower (Fig. 7b). These two findings might suggest that there is higher variability in the distribution of network activity patterns in *Cntnap2*$^{-/-}$ mice. We therefore quantified both single-cell and population variability in

baseline neuronal activity in the two genotypes. We found that the Fano factor (FF) values of spiking regularity, a common measure for single neuron noise, were similar in both genotypes (Fig. 7b). To quantify the variability of population baseline activity, we generalized the notion of spike rate variance and calculated the average changes in the population vector of firing patterns over time, as a measure of the nature of diffusion (or random walk) of the population[38,39]. This measure of baseline population noise was significantly higher in *Cntnap2*$^{-/-}$ mice compared with their WT littermates, in contrast to the FF values of single units (Fig. 7b). Of note, neither the elevated population noise nor the higher baseline FRs were correlated with mouse locomotion (Linear regression, for locomotion as predictor of FR: $F_{Cntnap2\text{-}/\text{-}(1,9)} = 0.168$, $P = 0.692$, $R^2 = 0.018$. $F_{WT(1,8)} = 0.165$ $P = 0.695$, $R^2 = 0.02$. For locomotion as predictor of population noise: $F_{Cntnap2\text{-}/\text{-}(1,9)} = 0.184$, $P = 0.678$. $R^2 = 0.02$. $F_{WT(1,8)} = 0.613$ $P = 0.456$, $R^2 = 0.071$).

We next tested whether these features of baseline activity could predict the SDI values describing the differential representation of social and nonsocial cues in the mPFC code. On the first day of stimulus presentation, none of the four features we examined were correlated with the SDI values (Fig. 7c. FR: r = -0.17, $t_{(9)} = -0.518$, P = 0.616; pairwise correlations: r = 0.223, $t_{(9)} = 0.686$, P = 0.511; FF: r = -0.458, $t_{(9)} = -1.546$, P = 0.156; Population noise: r = -0.287, $t_{(9)} = -0.9$, P = 0.392). On the second recording day, however, higher population noise levels were strongly indicative of smaller separation between social and nonsocial mPFC representations across mice and genotypes (Fig. 7c, r = -0.875, $t_{(9)} = -5.416$, $P = 4.24 \times 10^{-4}$). Importantly, population noise was the sole feature that was significantly correlated with the SDI values (FR: r = -0.529, $t_{(9)} = -1.87$, P = 0.094; pairwise correlations: r = -0.062, $t_{(9)} = 0.186$, P = 0.857; FF: r = -0.571, $t_{(9)} = -2.087$, P = 0.067). Moreover, population noise levels were also predictive of the change in SDI values between recording sessions, across individual mice (ΔSDI, Fig. 7d; r = -0.846, $t_{(9)} = -4.751$, P = 0.001). Thus, these findings suggest that elevated noise levels are predictive of decreased experience-dependent refinement of mPFC social representations.

Discussion

In this study, we investigated the neural encoding of social signals in the PFC of freely behaving mice. We found robust tuning to social stimuli in the mPFC unit activity and distinct population responses to social versus nonsocial signals. Repeated exposure of mice to the same set of cues revealed experience-dependent refinement of these representations between days. Consistent with previous reports of processing of salient sensory signals in the mPFC[40,41], we found that stimulus category (social/nonsocial), rather than individual odor identity, is predominantly represented in the mPFC neural code. Recent studies exploring stimulus encoding in olfactory cortical regions reported no difference in single-cell or population responses to social versus nonsocial odors[42], and showed concentration-invariant coding in the piriform cortex[43]. While our findings in the mPFC obey this concentration-invariance of odor responses, they are distinct in that social odors are more prominently represented at the single unit and neuronal population level. This social categorization therefore signifies an additional tier of processing in the mPFC. This process possibly relies on converging information from odor-driven activity in several long-range synaptic inputs to this region (for example, the piriform cortex or the orbitofrontal cortex[44,45]), and on inputs from brain regions encoding social context and incentive salience, such as the amygdala, the ventral tegmental area and the ventral hippocampus[44]. As the PFC is known to encode stimulus saliency[40,41], the observed social categorization might incorporate the innately rewarding properties of social stimuli[46].

Examining the responses to sensory cues across two separate recording sessions, we found that population activity patterns underwent significant refinement in WT mice. These findings expand upon recent work describing experience-dependent divergence of conspecific sex representations in the hypothalamus[47] and the medial amygdala[48]. In contrast to these regions, in which representations of sex specific signals diverge with behavioral experience, population activity in the mPFC seems to categorize cues based on their social or nonsocial nature, and this contrast is further refined with experience, whereas the representations of odors within each category, including between male and female cues, grow similar with time.

Our findings further show that mPFC activity in the *Cntnap2*$^{-/-}$ mouse model of autism displays reduced selectivity to social stimuli and loss of social categorization, while retaining information about the identity of individual odors. Our behavioral analysis demonstrated that while *Cntnap2*$^{-/-}$ mice display impaired social approach behavior, both toward live conspecifics and toward the social odors presented in this study, they show no impairment in their immediate sniffing

responses of the odors used in this study. Together with their intact performance in an olfactory-guided food-finding task, this indicates that *Cntnap2* mutants have intact olfactory sensing. In line with our findings, a recent study demonstrated that optogenetic excitation of parvalbumin-expressing inhibitory neurons in the mPFC of *Cntnap2*$^{-/-}$ mice leads to restoration of social behavioral responses[49], which suggests that the behavioral deficits in *Cntnap2*$^{-/-}$ mice do not arise form a primary sensory deficit, and may be intimately linked with the altered mPFC representations we observe here.

Most strikingly, *Cntnap2*$^{-/-}$ mice lacked the robust experience-dependent changes observed in the mPFC population code of WT mice. Impairments in short and long-term plasticity processes were previously described in both human ASD patients[30,31] and animal models of the disorder[32], but were not explored at the circuit level, or linked to the neuronal representation of social information. The loss of experience-based refinement of odor category representations in *Cntnap2*$^{-/-}$ mice might be linked with the role of the CNTNAP2 protein in targeting AMPA receptors to post-synaptic membranes[50]. Recent work demonstrated that there are reduced dendritic spine and synapse densities in the mPFC of *Cntnap2*$^{-/-}$ mice[16], thus providing a potential mechanism for the functional impairments we describe. The loss of these circuit-level plasticity processes in *Cntnap2*$^{-/-}$ mice might contribute to reduced selectivity in the mPFC representation of salient social cues and constitute a potential neuronal mechanism for the social impairment displayed by these mice.

Which network-wide changes might underlie these deficits? Our findings of elevated FRs, altered correlation structure and "noisy" baseline neuronal activity in *Cntnap2*$^{-/-}$ mice are consistent with several studies reporting changes in the E/I balance ratio, altered synaptic connectivity, disruption of dendritic morphology and population activity patterns in cortical circuits of this mouse model[18,36]. A low signal-to-noise ratio and increased response variability were previously reported in humans with ASD[21], but were not characterized at the level of spontaneous population activity in mouse models of the disorder. The strong negative correlation we observe between baseline population activity noise and social category representations suggests that noise plays an important role in the failure of mPFC activity in *Cntnap2*$^{-/-}$ mice to appropriately represent social cues and drive corresponding synaptic plasticity processes. These deficits might lead to an impaired ability to adaptively respond to relevant cues during social interactions. Taken together, our results present new insights into the encoding of social

information in the mPFC, and provide a neurophysiological perspective on the association between ongoing neocortical dynamics, stimulus processing and social dysfunction in autism.

Acknowledgements

This work was supported by grants from the Simons Foundation, the European Research Council (ERC 819496 PrefrontalMap, and ERC 311238 NEURO-POPCODE), the Israel Science Foundation, the Israel-US Binational Science Foundation, the Adelis Foundation, the Lord Sieff of Brimpton Memorial Fund and the Candice Appleton Family Trust. O.Y. is supported by a NARSAD Young Investigator Grant from the Brain & Behavior Research Foundation and by the Gertrude and Philip Nollman Career Development Chair. E.S. is the incumbent of the Joseph and Bessie Feinberg Professorial Chair.

Author contributions

D.R.L. and O.Y. designed the study, D.R.L. and A.W. built the experimental setup, D.R.L. performed all experiments and analyzed unit activity and behavioral data. A.P. and D.R.L. performed the sniffing experiments and analysis. D.R.L., T.T., O.Y., and E.S. performed population coding analyses. M.K. contributed to behavioral data analysis. D.R.L., O.Y., T.T., and E.S. wrote the manuscript.

Competing interests

The authors declare no competing interests.

References

1. Anderson, D. J. Circuit modules linking internal states and social behavior in flies and mice. *Nat. Rev. Neurosci.* **17**, 692‑704 (2016).
2. Chen, P. & Hong, W. Neural circuit mechanisms of social behavior. *Neuron* **98**, 16‑30 (2018).
3. Euston, D. R., Gruber, A. J. & McNaughton, B. L. The role of medial prefrontal cortex in memory and decision making. *Neuron* **76**, 1057‑1070 (2012).
4. Adolphs, R. The social brain: neural basis of social knowledge. *Annu. Rev. Psychol*. **60**, 693‑716 (2009).
5. Bicks, L. K., Koike, H., Akbarian, S. & Morishita, H. Prefrontal cortex and social cognition in mouse and man. *Front. Psychol.* **6**, 1‑15 (2015).
6. Watson, K. K. & Platt, M. L. Social signals in primate orbitofrontal cortex. *Curr. Biol.* **22**, 2268‑2273 (2012).
7. Zhou, T. et al. History of winning remodels thalamo‑PFC circuit to reinforce social dominance. *Science* **357**, 162‑168 (2017).
8. Murugan, M. et al. Combined social and spatial coding in a descending projection from the prefrontal cortex. *Cell* **171**, 1663‑1677.e16 (2017).
9. Lee, E. et al. Enhanced neuronal activity in the medial prefrontal cortex during social approach behavior. *J. Neurosci.* **36**, 6926‑6936 (2016).
10. Rigotti, M. et al. The importance of mixed selectivity in complex cognitive tasks. *Nature* **497**, 585‑590 (2013).
11. Parthasarathy, A. et al. Mixed selectivity morphs population codes in prefrontal cortex. *Nat. Neurosci.* **20**, 1770‑1779 (2017).
12. Zikopoulos, B. & Barbas, H. Changes in prefrontal axons may disrupt the network in autism. J*. Neurosci.* **30**, 14595‑14609 (2010).
13. Oblak, A., Gibbs, T. T. T. & Blatt, G. J. J. Decreased GABAA receptors and benzodiazepine binding sites in the anterior cingulate cortex in autism. *Autism Res.* **2**, 205‑219 (2009).
14. Carper, R. A. & Courchesne, E. Localized enlargement of the frontal cortex in early autism. *Biol. Psychiatry* **57**, 126‑133 (2005).
15. Rubenstein, J. L. R. & Merzenich, M. M. Model of autism: increased ratio of excitation/inhibition in key neural systems. *Genes Brain Behav.* **2**, 255‑267 (2003).
16. Lazaro, M. T. et al. Reduced prefrontal synaptic connectivity and disturbed oscillatory population dynamics in the CNTNAP2 model of autism. *Cell Rep.* **27**, 2567‑2578.e6 (2019).
17. Antoine, M. W., Langberg, T., Schnepel, P. & Feldman, D. E. Increased excitation‑inhibition ratio stabilizes synapse and circuit excitability in four autism mouse models. *Neuron* **101**, 648 661.e4 (2019).
18. Rubin, R., Abbott, L. F. & Sompolinsky, H. Balanced excitation and inhibition are required for high-capacity, noise-robust neuronal selectivity. *Proc. Natl Acad. Sci. USA* **114**, E9366‑E9375 (2017).
19. Scott-Van Zeeland, A. A. et al. Altered functional connectivity in frontal lobe circuits is associated with variation in the autism risk gene CNTNAP2. *Sci. Transl Med.* **2**, 56ra80 (2010).
20. Baum, S. H., Stevenson, R. A. & Wallace, M. T. Behavioral, perceptual, and neural alterations in sensory and multisensory function in autism spectrum disorder. *Prog. Neurobiol.* **134**, 140‑160 (2015).
21. Dinstein, I. et al. Unreliable evoked responses in autism. *Neuron* **75**, 981‑991 (2012).

22. Peñagarikano, O. et al. Absence of CNTNAP2 leads to epilepsy, neuronal migration abnormalities, and core autism-related deficits. *Cell* **147**, 235‑246 (2011).
23. Stowers, L. & Kuo, T.-H. Mammalian pheromones: emerging properties and mechanisms of detection. *Curr. Opin. Neurobiol.* **34**, 103‑109 (2015).
24. Root, C. M., Denny, C. A., Hen, R. & Axel, R. The participation of cortical amygdala in innate, odour-driven behaviour. *Nature* **515**, 269‑273 (2014).
25. Kobayakawa, K. et al. Innate versus learned odour processing in the mouse olfactory bulb. *Nature* **450**, 503‑508 (2007).
26. Schneidman, E., Berry, M. J., Segev, R. & Bialek, W. Weak pairwise correlations imply strongly correlated network states in a neural population. *Nature* **440**, 1007‑1012 (2006).
27. Granot-Atedgi, E., Tkačik, G., Segev, R. & Schneidman, E. Stimulusdependent maximum entropy models of neural population codes. *PLoS Comput. Biol.* **9**, e1002922 (2013).
28. Tkacik, G., Granot-Atedgi, E., Segev, R. & Schneidman, E. Retinal metric: a stimulus distance measure derived from population neural responses. *Phys. Rev. Lett.* **110**, 058104 (2013).
29. Alarcon, M. et al. Linkage, association, and gene-expression analyses identify CNTNAP2 as an autism-susceptibility gene. *Am. J. Hum. Genet.* **82**, 150‑159 (2008).
30. Bourgeron, T. From the genetic architecture to synaptic plasticity in autism spectrum disorder. *Nat. Rev. Neurosci.* **16**, 551‑563 (2015).
31. Guiraud, J. A. et al. Differential habituation to repeated sounds in infants at high risk for autism. *Neuroreport* **22**, 845‑849 (2011).
32. Auerbach, B. D., Osterweil, E. K. & Bear, M. F. Mutations causing syndromic autism define an axis of synaptic pathophysiology. *Nature* **480**, 63‑68 (2011).
33. Liska, A. et al. Homozygous loss of autism-risk gene CNTNAP2 results in reduced local and long-range prefrontal functional connectivity. *Cereb. Cortex* **28**, 1141‑1153 (2018).
34. Dickinson, A., Jones, M. & Milne, E. Measuring neural excitation and inhibition in autism: different approaches, different findings and different interpretations. *Brain Res.* **1648**, 277‑289 (2016).
35. Nelson, S. B. & Valakh, V. Excitatory/inhibitory balance and circuit homeostasis in autism spectrum disorders. *Neuron* **87**, 684‑698 (2015).
36. Litwin-Kumar, A. & Doiron, B. Slow dynamics and high variability in balanced cortical networks with clustered connections. *Nat. Neurosci.* **15**, 1498‑1505 (2012).
37. Shadlen, M. N. & Newsome, W. T. The variable discharge of cortical neurons: implications for connectivity, computation, and information coding. *J. Neurosci.* **18**, 3870‑3896 (1998).
38. Gerstein, G. L. & Mandelbrot, B. Random walk models for the spike activity of a single neuron. *Biophys. J.* **4**, 41‑68 (1964).
39. Stella, F., Baracskay, P., O' Neill, J. & Csicsvari, J. Hippocampal reactivation of random trajectories resembling Brownian diffusion. *Neuron* **102**, 450‑461.e7 (2019).
40. Otis, J. M. et al. Prefrontal cortex output circuits guide reward seeking through divergent cue encoding. *Nature* **543**, 103‑107 (2017).
41. Milad, M. R. & Quirk, G. J. Neurons in medial prefrontal cortex signal memory for fear extinction. *Nature* **420**, 70‑74 (2002).
42. Iurilli, G. & Datta, S. R. Population coding in an innately relevant olfactory area. *Neuron* **93**, 1180‑1197.e7 (2017).
43. Bolding, K. A. & Franks, K. M. Recurrent cortical circuits implement concentration-invariant odor coding. *Science* **361**, eaat6904 (2018).

44. Vertes, R. P. Differential projections of the infralimbic and prelimbic cortex in the rat. *Synapse* **51**, 32‑58 (2004).
45. Price, J. L. et al. in *Olfaction: A Model System for Computational Neuroscience* (eds Davis, J. L. & Eichenbaum, H.) 101‑120 (MIT Press, 1991).
46. Beny, Y. & Kimchi, T. Innate and learned aspects of pheromone-mediated social behaviours. *Anim. Behav.* **97**, 301‑311 (2014).
47. Remedios, R. et al. Social behaviour shapes hypothalamic neural ensemble representations of conspecific sex. *Nature* **550**, 388‑392 (2017).
48. Li, Y. et al. Neuronal representation of social information in the medial amygdala of awake behaving mice. *Cell* **171**, 1176‑1190.e17 (2017).
49. Selimbeyoglu, A. et al. Modulation of prefrontal cortex excitation/inhibition balance rescues social behavior in CNTNAP2-deficient mice. *Sci. Transl Med.* **9**, eaah6733 (2017).
50. Varea, O. et al. Synaptic abnormalities and cytoplasmic glutamate receptor aggregates in contactin associated protein-like 2 /Caspr2 knockout neurons. *Proc. Natl Acad. Sci. USA* **112**, 6176‑6181 (2015).

Figures

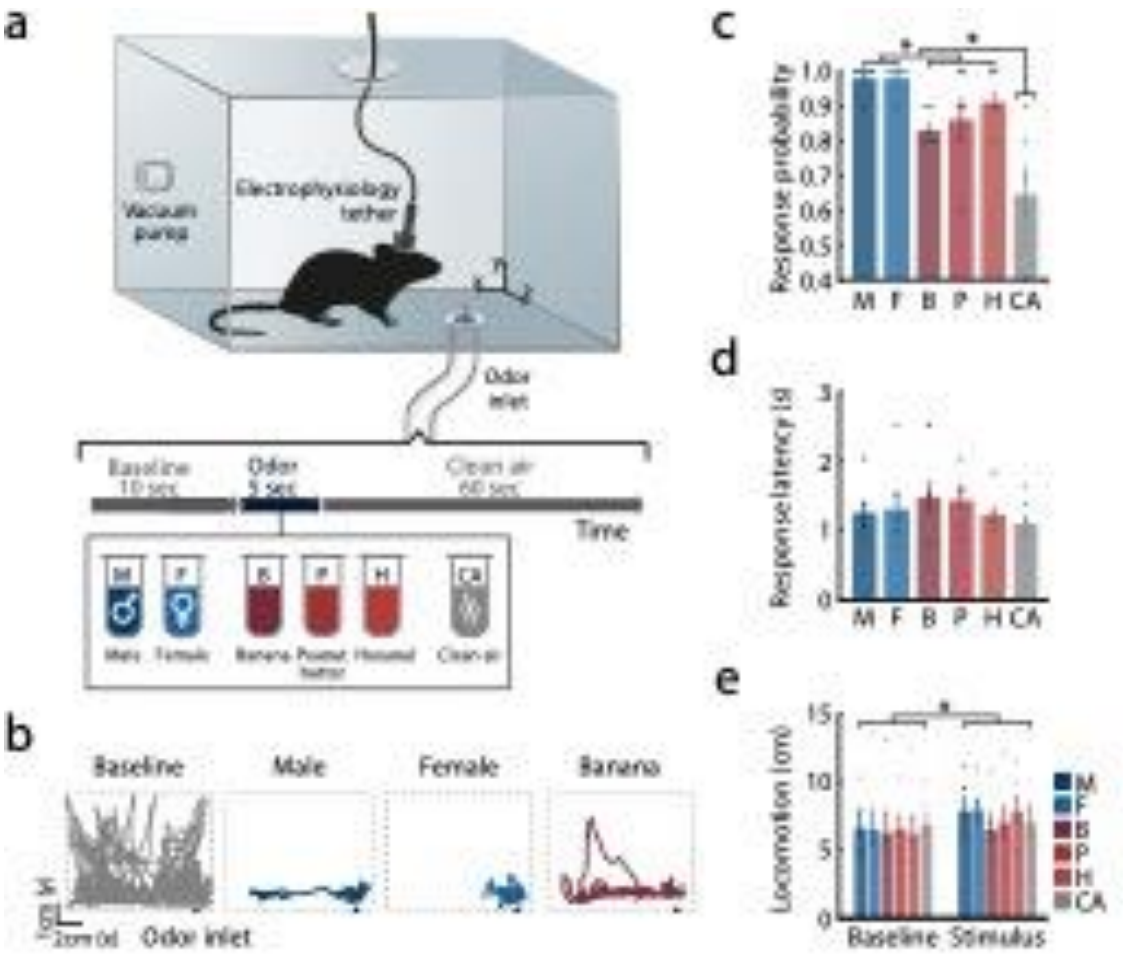

Fig. 1. Experimental setup for presentation of social and nonsocial olfactory cues to freely behaving mice.

a, Schematic representation of the experimental chamber and trial design. Freely behaving male mice were presented with social and nonsocial olfactory cues. Odors were presented in a pseudorandom order, interleaved with control trials in which only clean air was presented. All trials were preceded and followed by a constant infusion of clean air. Electrophysiological data were continuously recorded from the mPFC. The letters used for abbreviating the odors are applicable for all figures. **b**, Representative side-view trajectories of mouse locomotion during pre-stimulus baseline periods (gray) and during stimulus presentations (color). **c**, Probability of odor-evoked orientation responses across all odors. Friedman test for comparison of all stimuli,

$\chi^2_{(5)}$ = 21.235, P = 7.3x10^{-4}; Friedman test with post hoc two-sided Wilcoxon signed-ranked test for social, nonsocial and clean air comparison, $\chi^2_{(2)}$ = 12.0, P = 0.002; statistical significance of post hoc analysis is marked on the figure (mean response probability: social = 98.33 ± 1.05, nonsocial = 87.22 ± 3.03, clean air = 65 ± 7.63). **d**, Mean latency to odor-evoked orientation responses. Friedman test, $\chi^2_{(5)}$ = 1.809, P = 0.874. **e**, Locomotion during 5 s of stimulus presentation and during the corresponding pre-stimulus baseline periods. Two-way repeated-measures (RM) ANOVA, $F_{phase(1,5)}$ = 8.151, P = 0.036; $F_{stimulus(5,25)}$ = 0.387, P = 0.853; $F_{phaseXstimulus(5,25)}$ = 0.822, P = 0.546. Color code represents stimulus identity; circles mark individual mice. Data are presented as the mean ± s.e.m. (error bars), n = 6 mice, *P < 0.05. For detailed statistics information, see Supplementary Table 2.

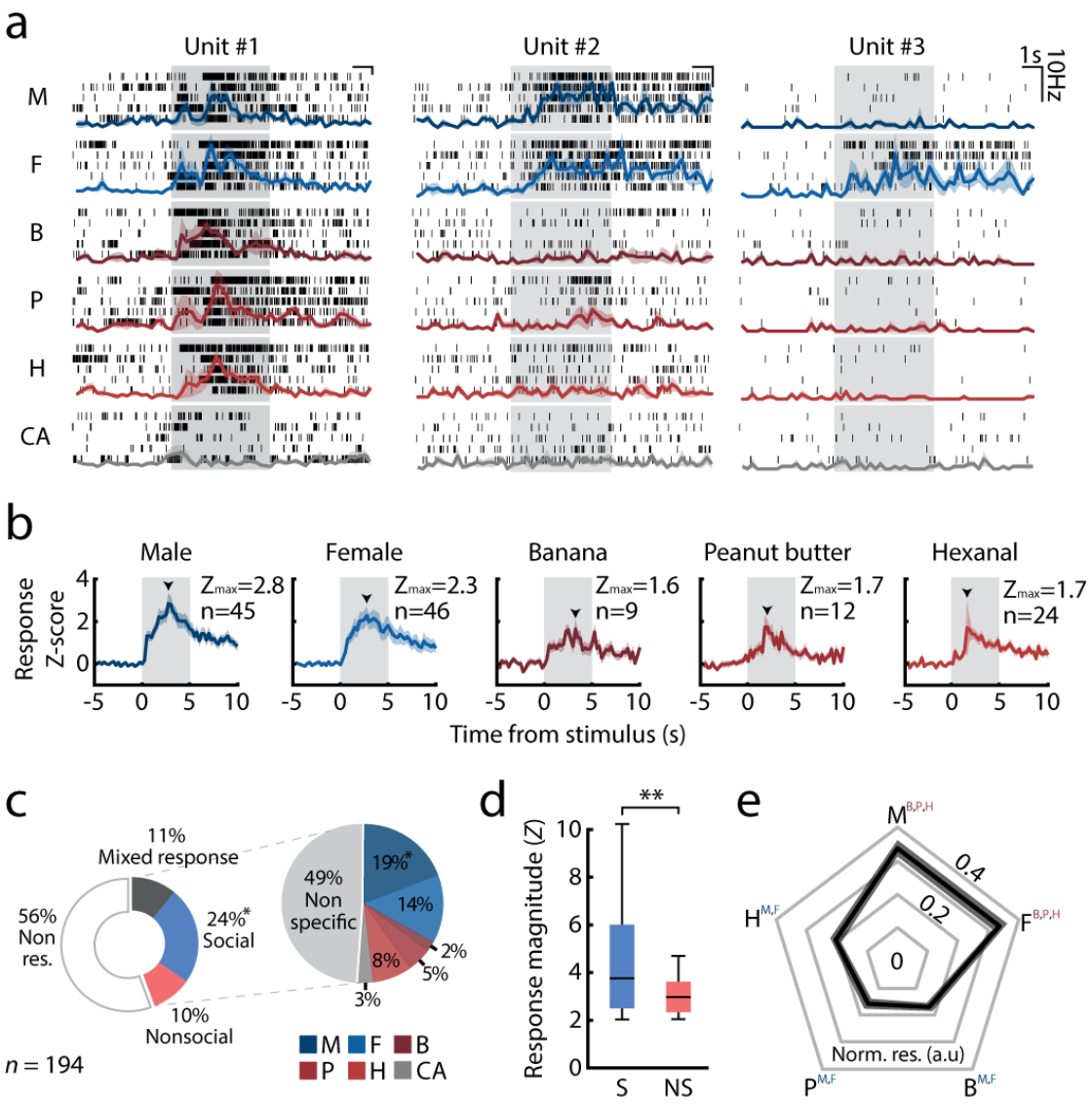

Fig. 2. Social tuning in mPFC unit response.

a, Representative evoked response patterns of mPFC single units to repeated presentations of odor stimuli. Shown are representative examples of units responding to all stimuli (left), social stimuli (middle, selective for M and F odors) and to a single stimulus (right, selective for F odor). Raster plots of unit responses are overlaid with the PSTH, normalized to the baseline FR of each unit (colored lines, in 250-ms bins). Shaded areas mark stimulus presentation time. The *y* scale bar refers to the PSTH. **b**, Stimulus-evoked PSTHs portraying the mean increase in FR of cue-responsive units (calculated as the response *Z*-score in 250-ms bins). Arrowheads mark the time of peak response. The mean peak response and number of responsive units are marked on individual panels. Shaded areas mark stimulus presentation times. **c**, Distribution of response

selectivity of all recorded units (left) and stimulus specificity among cue-responsive units (right). Colors represent stimulus identity. Left: $\chi^2_{(3)} = 15.793$, $P = 0.001$. Right: $\chi^2_{(5)} = 21.182$, $P = 7.5\text{x}10^{-4}$. Standardized residual analysis was used to determine significantly different response categories (|standardized residual| > 2), $n = 194$ units. **d**, Magnitude of stimulus-evoked response to social ($n = 91$ trial-averaged unit responses) versus nonsocial stimuli ($n = 46$ trial-averaged unit responses) calculated as the Z-scored increase in FR over 5 s of stimulus presentation. Two-sided Student's t-test, $t_{(103.4)} = 3.295$, $P = 0.001$. Box plot marks the interquartile range (IQR) and median, whiskers mark ± 1.5 X IQR. **e**, The mean normalized response magnitude to all stimuli across all responsive units ($n = 86$ units, see Methods). Superscript letters represent significant pairwise comparisons, determined by RM ANOVA with Bonferroni correction for post hoc comparisons. $F_{(4, 340)} = 27.427$, $P = 9.57\text{x}10^{-20}$. For all panels, data represent the mean ± s.e.m. (shaded area/error bars), *$P < 0.05$, **$P < 0.01$. For detailed statistics information, see Supplementary Table 2. a.u., arbitrary units; Non. res., non-responsive; Norm. res., normalized response.

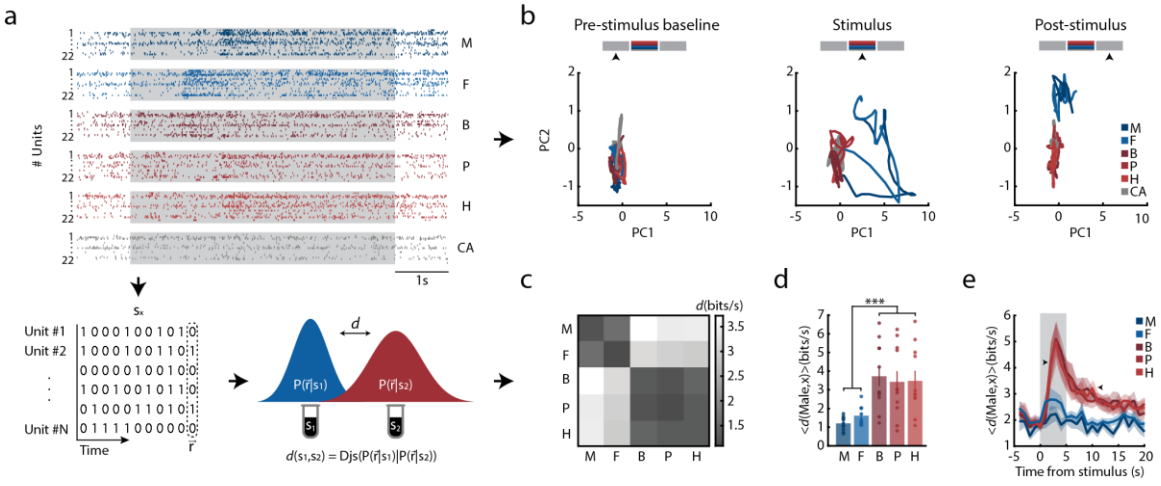

Fig. 3. Distinct representation of social cues in the mPFC neuronal population code.

a, Schematic illustration of the population analysis. Top: responses of multiple units recorded during a single recording session to each of the presented stimuli. Response patterns were used for neural trajectory analysis (as binned spike counts; **b**), and binarized in finer time bins for modeling the probability distribution of response patterns and response dissimilarity (bottom; **c**–**e**). **b**, Representative two-dimensional (2D) projections of the neuronal population trajectories

before, during and after stimulus presentation (each trajectory spans 5 s, where each point was estimated in 150-ms bins, n = 15 units; see Methods). The schemes above the panels indicate the corresponding phase along the trial. Colors represent odor identity. Here the first two PCs accounted for 75% of the variance. **c**, Similarity matrix depicting the population-based representation distance between each pair of stimuli, calculated over the final 2.5-s window of stimulus presentation. The block diagonal structure of the matrix indicates a clear divergence between social and nonsocial categories in the recorded mPFC activity. **d**, Distances between population responses to male cues and all stimuli (including the 'self-distance' between responses to male odor on different trials). Bars correspond to the first row or column in the matrix in **c**. Circles depict individual recording sessions (n = 11 sessions recorded from 6 mice). RM ANOVA with Bonferroni-corrected post hoc comparisons. $F_{stimulus(4,40)}$ = 16.255, P = 5.53x10^{-8}. **e**, Time-dependent distance of all stimulus representations from male cue responses, calculated in consecutive 1-s windows. Shaded gray area represents cue delivery time. Two-way RM ANOVA (for M, F and nonsocial stimuli) was performed with Dunnett's comparisons for each stimulus against its last baseline bin. $F_{stimulusXtime(40, 400)}$ = 3.84, P = 2.23x10^{-12}; $F_{stimulus(2,20)}$ = 29.794, P = 1x10^{-6}; $F_{time(20, 200)}$ = 5.665, P = 1.71x10^{-11} (n = 11 sessions recorded from 6 mice). Arrowheads mark range of post hoc statistical significance for nonsocial stimuli. For all panels, data represent the mean $\pm$ s.e.m. (shaded areas and error bars). ***P < 0.001. For detailed statistics information, see Supplementary Table 2.

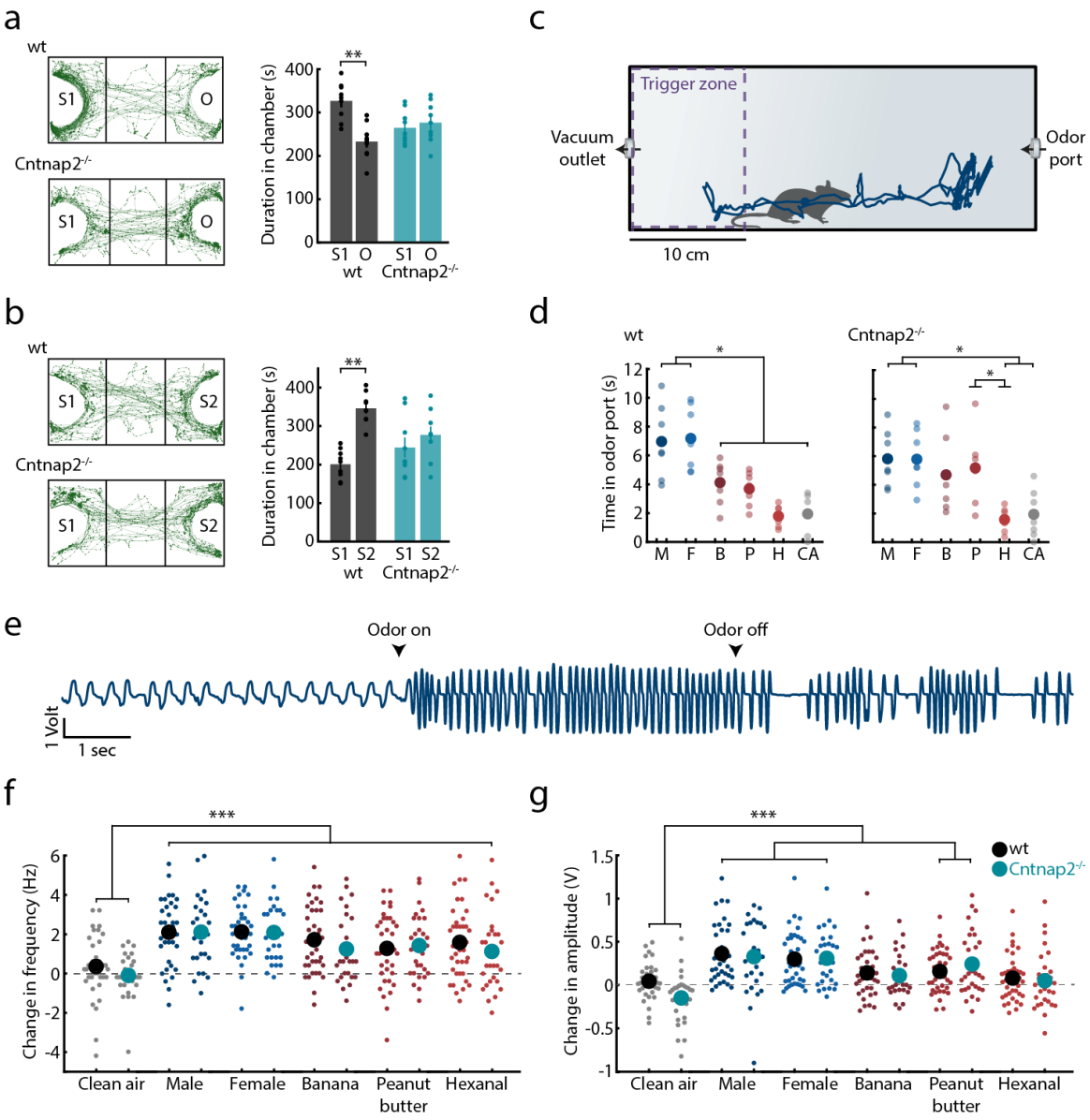

Fig. 4. *Cntnap2*$^{-/-}$ mice display impaired social behavior, but intact olfaction.

a, Three-chamber social preference test. Left: representative tracking traces for a single social preference trial of WT and *Cntanp2*$^{-}$/$^{-}$ mice (top view of set up). Right: average duration in the social (S1) and object (O) chambers for WT (n = 9) and *Cntnap2*$^{-/-}$ (n = 9) mice. Mixed-design RM ANOVA with post hoc Bonferroni correction. $F_{genotype(1,16)}$ = 5.97, P = 0.026; $F_{chamber(1,16)}$ = 4.39, P = 0.052; $F_{genotypeXchamber(1,16)}$ = 7.32, P = 0.015. **b**, Three-chamber social novelty preference test, testing for approach toward a familiar (S1) versus a novel (S2) conspecific. Traces (left) depict the same representative mice as in **a**. $F_{genotype(1,16)}$ = 5.257, P = 0.035; $F_{chamber(1,16)}$ = 11.144, P = 0.004;

$F_{genotypeXchamber(1,16)}$ = 4.84, P = 0.05. **c**, Schematic illustration of experimental chamber for the odor approach test (side-view, see Methods). Trial initiation zone is marked by the dashed purple line. Line marks representative automated tracking of mouse CoM (blue trace) during infusion of male odor. **d**, Mean duration of odor exploration, calculated as time sniffing odor port for WT (left, n = 7) and *Cntnap2*$^{-/-}$ mice (right, n = 7). Mice presented here were previously exposed to odor repertoire (see Extended Data Fig. 5d). RM ANOVA with Bonferroni corrections. For WT: $F_{stimulus(5,30)}$ = 13.981, P = 4.36x10^{-7}; for *Cntnap2*$^{-/-}$: $F_{stimulus(5,30)}$ = 6.841, P = 2.3x10^{-4}. **e**, Representative sniffing signal for a single presentation of male odor (see Methods). Arrowheads indicate time of odor presentation. **f**, Stimulus-evoked change in sniffing frequency for each odor for WT (black, n = 3 mice) and *Cntnap2*$^{-/-}$ mice (teal, n = 3 mice). Circles mark single trials. For statistics, trial repetitions were averaged for each experimental session (n = 13 sessions). Mixed-design RM ANOVA with Bonferroni correction for post hoc comparisons. $F_{genotype(1,11)}$ = 0.537, P = 0.48; F = 15.749, P = 1.32x10^{-9}; $F_{genotypeXstimulus(5,55)}$ = 0.575, P = 0.719. **g**, Same as **f**, but for stimulus-evoked change in sniff amplitude. $F_{genotype(1,11)}$ = 0.066, P = 0.803; $F_{stimulus(5,55)}$ = 12.912, P = 2.55x10^{-8}; $F_{genotypeXstimulus(5,55)}$ = 1.685, P = 0.153. For all panels, color code represents stimulus identity; circles mark individual mice unless otherwise indicated. Data represent the mean $\pm$ s.e.m. (error bars). *P < 0.05, **P < 0.01, ***P < 0.001. For detailed statistics information, see Supplementary Table 2.

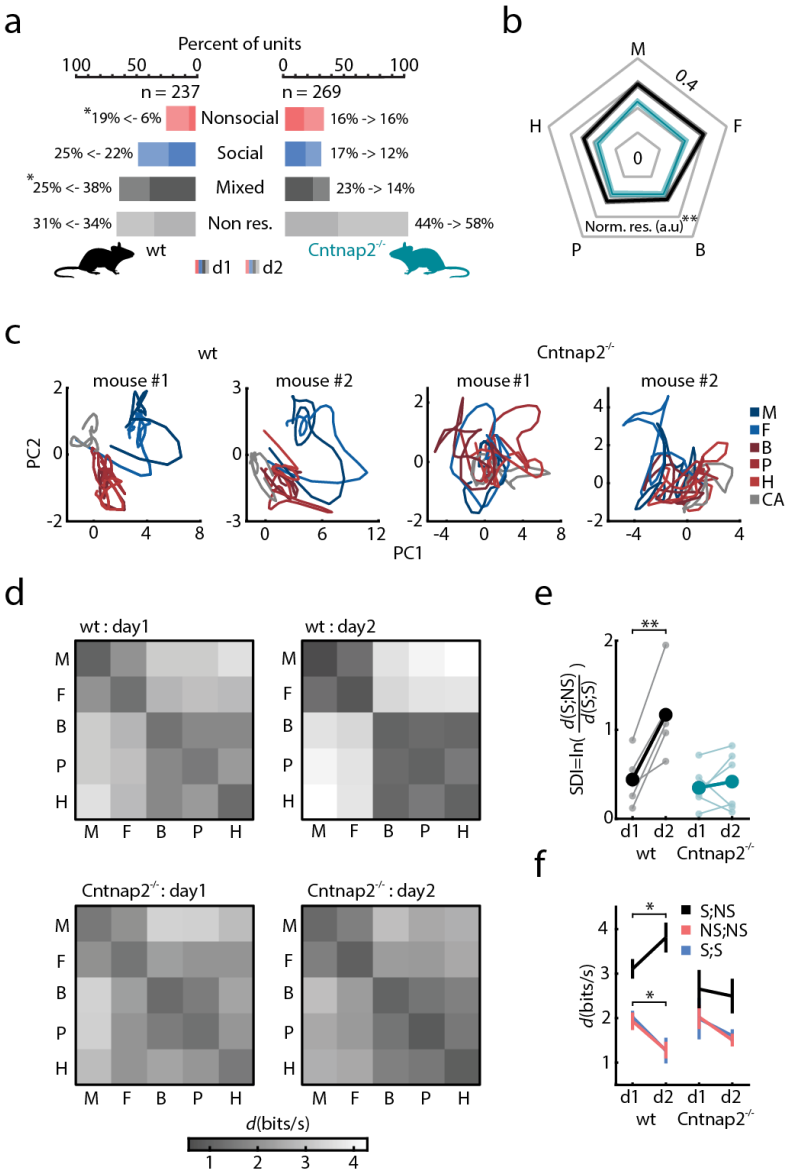

Fig. 5. Altered dynamics of social representation in the *Cntnap2*$^{-/-}$ mouse model of autism.

a, Distribution of response selectivity among WT (left) and *Cntnap2*$^{-/-}$ (right) mPFC units recorded in two consecutive recording sessions. Dark colors indicate distribution on day 1 (d1) of recording; light colors mark distribution on day 2 (d2). For WT, $n_{\text{day 1}}$ = 125 units, $n_{\text{day 2}}$ = 112 units recorded from 5 mice; for *Cntnap2*$^{-/-}$, $n_{\text{day 1}}$ = 133 units, $n_{\text{day 2}}$ = 136 units recorded from 6 mice. The change in percentage of units between days is marked on the figure. $\chi^2_{\text{WT(3)}} = 11.957$, $P = 0.008$; $\chi^2_{\text{Cntnap2}-/-(3)} = 6.789$, $P = 0.079$. Standardized residual analysis was used to determine post hoc significant changes in response categories between days (|standardized residual| > 2). **b**, Overall unit tuning, presented as the normalized response FR, for WT (left, n = 159 responsive units) and *Cntnap2*$^{-/-}$ mice (right, n = 131 responsive units). Mixed-design RM ANOVA with Bonferroni-corrected post

hoc comparisons. $F_{genotype(1,\ 288)}$ = 10.653, P = 0.001; $F_{stimulus(4,\ 1,152)}$ = 14.097, P = 3.1x10^{-11}; $F_{genotypeXstimulus(4,\ 1,152)}$ = 2.291, P = 0.058. Data represent the mean ± s.e.m. (shaded area). **c**, Representative 2D projection of population activity trajectories during stimulus presentation for two WT (left) and two *Cntnap2*$^{-/-}$ (right) mice during the second day of recording (for WT, $n_{mouse\ 1}$ = 22 units, $n_{mouse\ 2}$ = 31 units; for *Cntnap2*$^{-/-}$, $n_{mouse\ 1}$ = 17 units, $n_{mouse\ 2}$ = 27 units; see Methods). Colors represent odor identity. Here the first two PCs accounted for 74−82% of the variance. **d**, Similarity matrices depicting the distance between population responses to stimuli in WT (upper, n = 5) and *Cntnap2*$^{-/-}$ (lower, n = 6) mice, during the first (left) and second (right) recording days. **e**, Distance-based SDI (see the main text for details) for WT and *Cntnap2*$^{-/-}$ mice for two consecutive recording sessions. Higher index values indicate greater divergence between social and nonsocial stimuli. Bold lines depict mean values over mice, thin lines represent individual mice (n_{WT} = 5, $n_{Cntnap2\text{-}/\text{-}}$ = 6). Mixed-design RM ANOVA with Bonferroni corrections. $F_{genotypeXday(1,9)}$ = 14.05, P = 0.005; $F_{day(1,9)}$ = 20.586, P = 0.001; $F_{genotype(1,9)}$ = 5.14, P = 0.049. **f**, Average dissimilarity between odor-evoked responses (d) within categories (NS;NS and S;S) and between them (S;NS) for WT and *Cntnap2*$^{-/-}$ mice, over two consecutive recording sessions (n_{WT} = 5 mice, $n_{Cntnap2\text{-}/\text{-}}$ = 6 mice). Two-way RM ANOVA with Bonferroni-corrected post hoc comparisons. For WT: $F_{dissimilarityXday(2,8)}$ = 12.952, P = 0.003; $F_{dissimilarity(2,8)}$ = 34.723, P = 1x10^{-4}; $F_{day(1,4)}$ = 2.925, P = 0.162; For *Cntnap2*$^{-/-}$: $F_{dissimilarityXday(2,10)}$ = 0.5, P = 0.621; $F_{dissimilarity\ (2,10)}$ = 8.854, P = 0.006; $F_{day(1,5)}$ = 1.051, P = 0.352 (main effect of dissimilarity refers to differences between S;NS, NS;NS and S;S). For all panels, data represent the mean ± s.e.m. *P < 0.05, **P < 0.01. For detailed statistics information, see Supplementary Table 2.

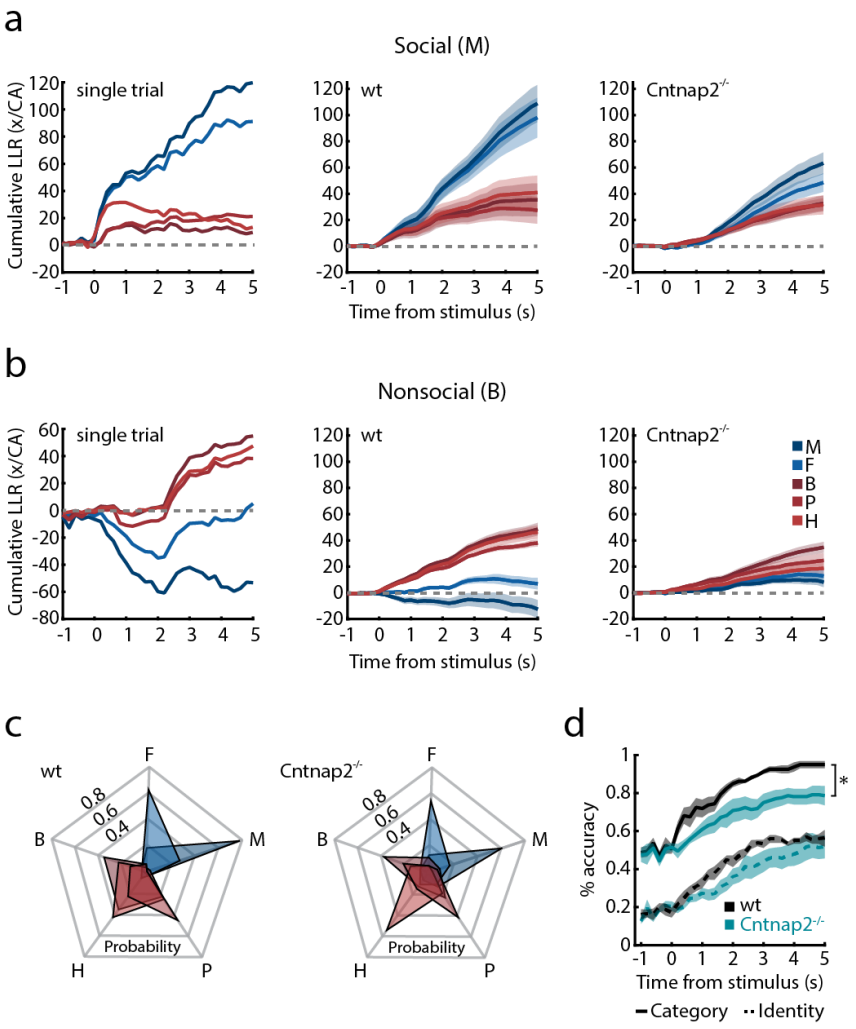

Fig. 6. Decoding of stimulus identity and social category from mPFC population code.

a, Left: an example of the time-dependent cumulative LLR of population responses to each stimulus and to clean air, on a single trial in which male odor was presented to a WT mouse. Middle: the average of the same LLR across all such trials over all WT mice (n = 5). Right: the average across all such trials over all *Cntnap2*$^{-/-}$ mice (n = 6). **b**, Time-dependent cumulative LLR of each stimulus in trials where banana odor was presented (all compared with CA; left: single-trial data; middle: average for WT mice; right: average for *Cntnap2*$^{-/-}$ mice). **c**, Decoding performance for individual stimuli in WT (left) and *Cntnap2*$^{-/-}$ (right) mice. Performance was summarized as the probability of classifying the presented stimulus as either one of all possible stimuli across all mice and trials. Colors mark correct odor classification; letters represent possible decoder responses. **d**, Cumulative accuracy of odor-based (dashed lines) and category-based (solid lines) decoders for WT (n = 5) and *Cntnap2*$^{-/-}$ (n = 6) mice. Comparison of maximal accuracy values between

genotypes: two-sided Mann–Whitney *U*-test for stimulus category: $U = 1$, $P = 0.009$; for stimulus identity: $U = 11$, $P = 0.537$. For all panels, data represent the mean ± s.e.m. $^{**}P < 0.01$.

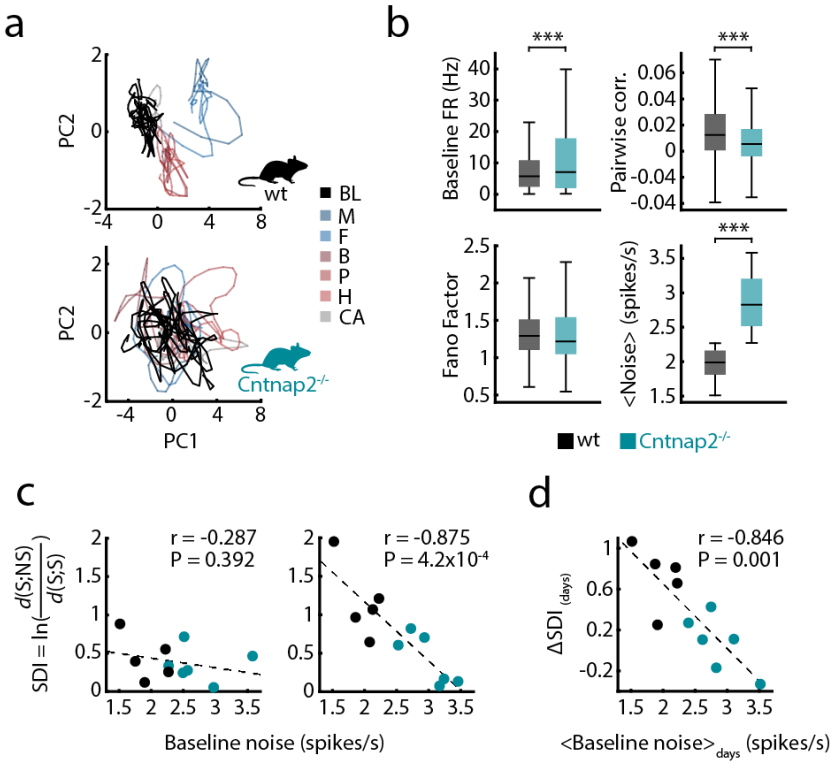

Fig. 7. Elevated neural noise correlates with deficits in social processing in *Cntnap2*$^{-/-}$ mice.

a, Representative 2D projection of neural trajectories of baseline (BL) activity (black line) in WT (top, $n = 22$ units) and *Cntnap2*$^{-/-}$ (bottom, $n = 17$ units) mice. Traces are overlaid on corresponding trajectories of stimulus-evoked activity in the same mice (light color lines; see also Fig. 5c). **b**, Comparison of unit and population properties in baseline (spontaneous) mPFC activity in WT ($n = 5$) and *Cntnap2*$^{-/-}$ ($n = 6$) mice. Two-sided Student's *t*-test with Bonferroni correction for multiple comparison were performed for all panels. For the FR of all recorded units (top left): $t_{(422.4)} = 3.903$, $P = 4.4\text{x}10^{-4}$, $n_{WT} = 230$ units, $n_{Cntnap2\text{-}/\text{-}} = 261$ units; for pairwise correlations (top right): $t_{(5447.3)} = 8.791$, $P = 1.95\text{x}10^{-18}$, $n_{WT} = 2{,}694$ pairs, $n_{Cntnap2\text{-}/\text{-}} = 2{,}798$ pairs; for FF (bottom left): $t_{(424.4)} = 1.563$, $P = 0.475$, $n_{WT} = 230$ units, $n_{Cntnap2\text{-}/\text{-}} = 261$ units; for baseline noise (bottom right): $t_{(20)} = 5.903$, $P = 3.59\text{x}10_{-5}$, $n_{WT} = 10$ recording sessions, $n_{Cntnap2\text{-}/\text{-}} = 12$ recording sessions (see Methods and **a** for 2D projection of this measurement). Box plot marks IQR and median, whiskers

mark ±1.5 x IQR. **c**, Pearson's correlation between baseline noise level and SDI values for WT (black) and *Cntnap2*$^{-/-}$ mice (teal), for the first (left) and second (right) recording sessions. Circles represent individual mice; Correlations were calculated across genotypes and corresponding values are marked on figure. **d**, Pearson's correlation between average population baseline noise levels and change in SDI values between recording days for WT and *Cntnap2*$^{-/-}$ mice. Correlation was calculated across genotypes and corresponding values are marked on the figure. For all panels, data represent the mean ± s.e.m. (note that some s.e.m. in **c** and **d** are smaller than the marker size). ***$P < 0.001$.

Methods

Animals

Animals used for this study were adult (3-6 months old) male C57BL/6J mice (Envigo, Rehovot, Israel), and adult (3-6 months old) *Cntnap2*$^{-/-}$ and *Cntnap2*$^{+/+}$ male littermates (courtesy of Prof. Elior Peles of the Weizmann Institute of Science). The *Cntnap2* knockout mice were previously back-crossed to a C57BL/6J background for at least 10 generations[22], and maintained by heterozygote breeding. Mice were kept on a 12-h light/dark cycle with food and water ad libitum, and tested during the dark phase. All mice were grouped housed (four mice in a cage) prior to surgical procedures. All procedures described in this paper were approved by the Weizmann Institute Animal Care and Use Committee (IACUC).

Stereotaxic surgery and microwire array implantation

Mice were anesthetized with an intraperitoneal injection of Ketamine–Xylazine mixture (80 mg/kg Ketamine, 10 mg/kg Xylazine), placed into a stereotaxic frame (David Kopf Instruments) and kept under 1.5% isoflurane anesthesia throughout the procedure. Microwire electrode arrays were implanted in the infralimbic region of the medial prefrontal cortex[51] (distance from Bregma: AP: +1.97; ML ±0.3 counter balanced between mice; DV -3.0), and secured to the skull using Metabond (Parkell) and dental acrylic. Analgesic (Buprenorphine, 0.05 mg/kg) was provided immediately post-surgery. Mice were placed in an individual cage and allowed 2-weeks to recover before initiation of experimental trials. Locations of implanted drives were validated in all experimental animals using an electrolytic lesion (see histology section below and Extended Data Fig. 1 c,d).

In-vivo electrophysiological recordings

Multi-electrode drive consisted of a graded electrode bundle of 16 microwires (25-µm diameter straightened tungsten wires; Wiretronic Inc.), attached to an 18-pin dual row connector (Mill-Max, Oyster Bay, NY). Unit signals were amplified using a HS-18-CNR-LED unity-gain headstage amplifier, filtered (600-6,000 Hz), digitized at 32 kHz and stored using the Digital Lynx hardware and Cheetah software acquisition system (Neuralynx Inc.).

Histology

Mice were deeply anesthetized using an intraperitoneal injection of Ketamine–Xylazine mixture (160 mg/kg Ketamine, 20 mg/kg Xylazine) and the locations of implanted electrodes were marked with electrolytic lesions (unipolar 100 μA current for 5 s, for each polarity). Twenty minutes following the lesion procedure, mice were further anesthetized using Pentobarbital (130 mg/kg^{-1}, i.p.), and then transcardially perfused with ice-cold phosphate buffered saline (PBS, pH 7.4) followed by 4% paraformaldehyde solution. Brains were extracted, post-fixed overnight at 4 °C in 4% PFA, and then moved to 30% sucrose solution for at least 48 hours. Coronal sections (35μm) were acquired using a microtome (Leica Microsystems) and collected in a cryoprotectant solution (25% glycerol, 30% ethylene glycol in PBS, pH 6.7). Sections were stained with a nucleic acid dye to better visualize lesion location (DAPI, 1:10,000), mounted on gelatin-coated slides, dehydrated and embedded in DABCO mounting medium (Sigma). Tiled overview images (X10) were acquired using a LSM 700 confocal microscope (Zeiss), and lesion locations were recorded.

Odor infusion apparatus

The apparatus consists of a transparent polycarbonate chamber (15cm X 10 cm X 15cm), connected to a custom-made 7-odor olfactometer plugged into a 1/8" odor inlet in the chamber floor. Odor stimuli were placed in individual polytetrafluoroethylene (PTFE) vials, each directed to the chamber through a separate tube system converging onto a designated PTFE hub at the inlet odor port. One-way check valves were placed in each odor path to prevent back-flow of odors.

Odors were infused via constant airflow stream directed through alternating solenoids controlled by a MOSFET Electronic driver. Odor alternation occurred within ~12ms (as measured using a pressure sensor, see Extended Data Fig. 1a). Air from the chamber was constantly cleared using a vacuum system in order to maintain constant pressure and clear odor residue throughout the experiment. In/out airflows were controlled using four 24VDC pressure pumps (Conlog Ltd. Israel) and fine-tuned using a built-in valve. The kinetics of odor concentration in the chamber were assessed using a VOC meter (MiniRAE Lite; RAE systems, San Jose CA. see Extended Data Fig. 1b). Odor concentrations showed a sharp increase immediately after stimulus onset, continued to increase throughout stimulus infusion, and slowly decreased back to baseline levels (a decrease of an order of magnitude in concentration was measured within ~60 seconds from stimulus off). All air pumps were isolated inside a sound attenuating box designed to minimize noise levels. All

pipes, inlets and odor tubes were either constructed of or coated with PTFE to prevent odor contamination.

The setup was back-lit with a planar infra-red (IR) LED array (880nm, 1Vision Ltd., Israel), allowing high-contrast recording and analysis of mouse behavior. The IR backlight was isolated from the behavioral chamber with a transparent conductive mask (Holland Shielding Systems B.V., the Netherlands) to minimize electrical noise in recorded channels. Two buffered 1.3MP monochromatic infrared triggered CMOS cameras (Mightex Systems), as well as the Neuralynx IR camera were used to record the experiment from a top and side view simultaneously, allowing for analysis of behavior with high-temporal resolution alongside the electrophysiological data. All components of the setup were controlled using a National Instruments data logger (NI USB-6353, National Instruments, Austin, TX), and a custom-written Matlab program. All events in the odor delivery setup were logged on the Neuralynx system using digital TTL inputs.

Odor stimuli and experimental procedure

Social cues consisted of soiled bedding and 50µl of urine collected and pooled from 10 male (M) or 10 female (F) adult C57BL/6J mice, in order to minimize the effect of individual cues between experimental repetitions. Nonsocial odor stimuli were: Banana (B) and Peanut butter (P) oil mixtures (Sensale, Ramat-Gan, Israel) and a monomolecular Hexanal (H) odorant (Sigma-Aldrich), all diluted 10^{-2} in double-distilled water on the morning of each experiment. When recording unit responses to varying concentrations (see Extended Data Fig. 3), banana oil mixture was diluted in double-distilled water to reach 1:50, 1:100 and 1:500 dilutions; soiled male bedding was mixed with clean bedding and male urine was diluted in saline to reach a final mixture ratio of 1:5 and 1:10 of the original male stimulus.

At the beginning of each experimental day, mice were connected to the electrophysiological tether and placed in the chamber for 15-30 minutes to allow habituation to the setup and stabilization of electrophysiological signals. The experimental procedure initiated with three minutes of baseline recording followed by odor presentation trials. Each trial consisted of 10 seconds of clean air, followed by 5 seconds of odor infusion and an additional 60 seconds of clean air infusion to clear the chamber of odor residue (see Fig. 1a). Each experiment consisted of 40 such trials (8 trials for each of the 5 selected stimuli: M/F/B/P/H) and 48 trials for the varied concentrations experiments (8 repetitions for each of the 6 presented odors). Trials were pseudo-randomized to prevent multiple consecutive presentations of a single odor, and interleaved with

eight additional clean air trials using the same trial design (to account for possible changes in airflow and sound due to solenoid switching). After the end of odor delivery trials, ongoing spontaneous activity was recorded for at least 5 additional minutes. Vacuum pump was constantly activated throughout the experiment (including habituation and baseline times), and clean air was constantly infused into the chamber with the exception of odor delivery times. All experiments were done under a dim ambient light of 3 Lux.

For C57BL/6J experiments, mice were repeatedly exposed to the odor stimuli prior to initiation of experiments. Mice were used for two recording session separated more than a month apart. For experiments involving *Cntnap2*$^{-/-}$ and *Cntnap2*$^{+/+}$ mice, mice were never before exposed to odor stimuli prior to the first experimental day. In this experiment, recording session were conducted 2 or 5 days apart, with inter-session gaps similarly distributed between the two groups.

Behavioral assays

Mice were acclimated to the behavioral room for two consecutive days prior to the initiation of behavioral trials. An additional habituation of one hour was performed on the morning of each experimental session. The order of trials was counterbalanced between days and between genotypes. Automated tracking of recorded videos was performed using EthoVision v13. software (Noldus Information Technology), or using custom Matlab scripts. Manual analysis of behaviors was performed using Observer XT v13 (Noldus Information Technology). All analyses were conducted by a trained observer, blind to mouse genotype. All assays were conducted during the dark phase and under dim red light, unless otherwise indicated.

Odor approach assay

Mice (n = 7 WT and n = 7 *Cntnap2*$^{-/-}$) were placed in an elongated odor infusion apparatus (35 cm X 10 cm X 15 cm) and allowed to freely explore the arena for 15 min prior to initiation of the experiment. Odor stimuli were as described above (see Odor stimuli and experimental procedure). Each odor was presented three times for 30 sec, in pseudo-randomized order with an inter-trial-interval of at least 120 sec from the previous odor presentation. Each mouse performed two experimental session separated one week apart. In order to maximize collection of behavioral parameters, online tracking of mouse location was conducted using the EthoVision software, and odor delivery triggers were controlled by input - output box, such that odors were infused only when the mouse was at least 25 cm away from odor port. Odor trials were interleaved with control trials in which only clean air was presented, and clean air was continuously infused into

the chamber during inter-trials-intervals. Mouse location was tracked automatically and sniffing duration (Time in port) was calculated for each odor presentation (see Automated behavioral analysis).

Three-chamber social assay

A three-chamber arena (52 cm X 26 cm X 23 cm, side chambers measured 20 cm X 26 cm X 22 cm, central compartment measured 12 cm X 26 cm X 23 cm) was constructed of clear Plexiglas covered with an opaque plastic cover. Mice (n = 9 WT and n = 9 *Cntnap2*$^{-/-}$ mice) were placed in the central compartment of and allowed 10 minutes to habituate to the arena. Mouse position was continuously recorded and automatically scored to exclude any pre-existing side preferences. Following the habituation phase, wire-mesh cages containing either a social stimulus (adult C57BL/6J male mouse, S1) or an object (two stacked 5 cm X 5 cm X 5 cm black cubes, O) were placed in the two opposing side chambers. Experimental mice were then allowed to explore the arena for an additional 10 minutes. The object stimulus was then replaced by a novel social stimulus (an adult C57BL/6J male mouse, S2), and mice were allowed to explore the arena for 10 additional minutes[52]. All stimulus mice were previously unfamiliar adult C57BL/6J male mice, habituated to the setup and mesh-wire cages for two consecutive days before the start of experimental sessions. Mice from different cages were used as familiar (S1) and novel (S2) social stimuli to ensure differential olfactory signals. The location of the social and object stimuli was counterbalanced between trials and genotypes. The position of the experimental mice was recorded and automatically tracked using the EthoVision 13.0 software.

Buried food find assay

Mice (n = 8 WT and n = 8 *Cntnap2*$^{-/-}$) were food-deprived for 18 hours prior to initiation of experiments. On the morning of the experimental day, mice were weighed to ensure ~10% weight loss (10.2 ± 0.27), and allowed 5 min to habituate to a large arena (42cm X 26cm X 18cm), covered with 3 cm of clean bedding. For food foraging assay, mice were gently removed from cage and a small food pellet (~1 gram) was hidden in a random location underneath the bedding. Mice were then gently placed back in the center of the chamber and allowed to freely forage for the hidden food[53]. All trials were recorded using a video camera, and latency to find the buried food was manually measured using a stopwatch and verified with offline video-based analysis. All mice recovered the hidden food palate within 150 sec of trial initiation.

Open field test

Mice (n = 8 WT and n = 8 *Cntnap2*$^{-/-}$) were gently placed in the center of a rectangular (50 cm X 50 cm X 50 cm), brightly lit opaque arena (~120 Lux, evenly illuminated), and allowed to freely explore their surroundings for 10 minutes. A 25 cm X 25 cm rectangle in the center of the arena was defined as "center". Mouse location and locomotion were recorded and automatically tracked using EthoVision 13.0 software.

Automated behavioral analysis

For analysis of behavior performed during electrophysiological recordings, recorded videos were automatically analyzed frame by frame, using custom-written MATLAB scripts (version 2017a, MathWorks, Natick, MA). Videos of experimental sessions were segmented using a fixed-threshold, and body contour was distinguished from the electrophysiology headstage and tether using erosion and dilation procedures. The center of mass (CoM) of the mouse was then determined for future analysis. Locomotion values were calculated by integrating the Euclidean distances (absolute values) between pairs of CoM values in consecutive frames, over a period of 5 s during odor presentation or immediately beforehand (for baseline measurements). The initial attention response and orientation to odor infusion were scored manually frame-by-frame. This data was then averaged per mouse (across trials and sessions) unless otherwise indicated. One mouse was excluded from behavioral analysis on a single recording session due to technical issue with the recorded video file. All analyses were conducted by a trained observer, blind to stimulus identity and mouse genotype.

For odor approach experiments, recorded videos were automatically analyzed using custom-written MATLAB scripts (version 2017b). Mouse center of mass (CoM) was extracted with single-frame resolution and used for tracking mouse location within the apparatus. The duration in odor port was defined as integration of times in which the animal's body covered at least 1/3 of pixels within a 0.7cm^2 rectangle around the odor port.

In-vivo sniffing assay

Cannula implantation

Mice were anesthetized in an induction chamber containing 4% isoflurane mix, placed into a stereotaxic frame and kept under 1.5% isoflurane anesthesia throughout the procedure. An incision was made to expose the nasal bone and a small hole was drilled to expose the nasal cavity.

A 7 mm-long stainless-steel cannula (23 gauge) was then inserted into the cavity and stabilized using dental acrylic (3M, Germany)[54]. The intranasal cannula was connected to a pressure sensor (24PCEFJ6G; Honeywell) using polyethylene tubing (801000; A-M Systems) and sniffing signals were visualized online using an oscilloscope. Mice which presented a clear sniff signal and no cannula obstruction were used in experiments. To prevent clogging, a 7.5 mm-long stainless-steel dummy cannula (26 gauge) was inserted into the cannula and was removed on experiment day.

Experimental procedure

Experimental mice (n = 3 WT and n = 3 *Cntnap2*$^{-/-}$) were placed in odor infusion box as described above. The experimental procedure, stimuli and all other parameters were as described for the electrophysiology experiments. Each odor was presented 5 times, and mice were recorded in 2 recording sessions spaced 1-3 days apart (with the exception of a single WT mice that was used in 3 recording session). Sniffing signals were recorded throughout the session as described below.

Sniffing detection and data analysis

Sniffing was detected as a change in air pressure in the intranasal cavity. Pressure changes were measured using a designated pressure sensor, placed outside the odor infusion box and connected to an intranasal cannula using polyethylene tubing. The length of the tube was optimized to allow the experimental mouse to behave freely within the odor infusion chamber. Changes in air pressure were amplified and recorded as an analog signal using a DAQ board (NI USB-6353, National Instruments, sampling rate 1KHz) that was also used to trigger odor infusion, allowing for automatic synchronization of recorded sniff signal and "odor on/off" events.

Sniffing signals were analyzed using a custom Matlab script. Analog data was initially smoothed (moving average, span = 10 ms), and normalized by subtraction of signal median calculated individually for each trial. Sniffing frequency and amplitude were calculated by automatic detection of signal peaks during 5 sec prior to stimulus presentation (baseline period) and 5 sec during stimulus presentation, for each trial. Trials in which cannula air flow was obstructed during baseline or stimulus times (~10%) were excluded from analysis.

Population activity modeling and analysis

To study population coding at a fine temporal resolution, we discretized population activity patterns into 20 ms bins, where the activity of the units at time bin *t* was given by a binary vector

$\vec{r}(t) = r_1(t), r_2(t), \ldots, r_N(t)$, where $r_i = 1(0)$ denotes whether neuron *i* spiked in that bin. Since estimating the encoding distribution $P(\vec{r}|s)$ directly from the data is impractical due to under-sampling (see Extended Data Fig. 4), we constructed for each time window a model $P_{model}(\vec{r}|s)$ of the distribution of neural responses as a function of time, based on the minimal models that have the correct firing rates of individual units, $\langle r_i(t) \rangle$, and pairwise correlations between them $\langle r_i(t) r_j(t) \rangle$ (where $\langle \quad \rangle$, denote average over time and over stimulus presentations) known as stimulus dependent maximum entropy models[27]. For each population recorded from each animal and for each stimulus, we fit two models: (1) the maximum entropy model based only on the time dependent firing rates, giving the conditionally independent population model,

$$P_{Indep}(\vec{r}|s) = \prod_i P(r_i|s),$$

which assumes no correlations between units, and (2) a stimulus-dependent second-order maximum entropy (ME2) model that also takes into account the time dependent correlations between units, as previously described[26,55]. The ME2 model is known to take the form:

$$P_{ME2}(\vec{r}|s) = \frac{1}{Z} \exp\left(\sum_i \alpha_i r_i + \sum_{i<j} \beta_{ij} r_i r_j\right),$$

where $\{\alpha_i, \beta_{ij}\}$ are Lagrange multipliers that were fit so that the averages $\{\langle r_i(t) \rangle, \langle r_i(t) r_j(t) \rangle\}$ of the model agree with experimental data, and *Z* is a normalization term or the partition function. We then estimated the likelihood of held out test data for each of the models, in order to choose the model which provided the best fit to the data (see Extended Data Fig. 4a). The chosen model was then used in the analysis of the neural population activity patterns. In all cases, the models gave a highly accurate description of the data, which was superior to those based on the empirically sampled responses (see Extended Data Fig. 4c). Despite the response habituation observed over repeated cue presentation for single unit responses, using subsampling of trials for construction population models (either early trials 1-4, or later trials 5-8) did not affect the population analysis results. All data modeling was performed using a designated Matlab-based toolbox[56].

Dissimilarity of stimulus-evoked encoding distributions

To quantify the dissimilarity of stimulus-evoked population activity patterns, the "distance" between two stimuli was quantified as the dissimilarity between their encoding distributions,

calculated by the Jensen-Shannon divergence[28,57]: $d(s_i, s_j) = D_{js}[P(\vec{r}|s_i)||P(\vec{r}|s_j)]$. The Jensen-Shannon divergence is a symmetrized version of the Kullbak-Leibler divergence, which measures in bits how distinguishable two distributions are, yielding 0 for identical distributions and 1 for non-overlapping distributions[58].

$$D_{js}(P||Q) = \frac{1}{2}D_{kl}(P||M) + \frac{1}{2}D_{kl}(Q||M), \;\; M = \frac{1}{2}(P+Q),$$

For each animal, the encoding distributions models were fit to 30 randomly selected groups of ten units. In order to evaluate self-distance (*d*(x,x)) we fit two models of the encoding distribution of each stimulus, using half of the trials (odd/even trials) as training data for each model, and then calculated the D_{js} between them: $d(s_i, s_i) = D_{js}[P_{odd}(\vec{r}|s_i)||P_{even}(\vec{r}|s_i)]$. A single mouse was removed from this analysis (presented in Fig. 3c-e) due to insufficient number of simultaneously recorded units (7 units).

Neural trajectory analysis and baseline activity calculations

For analysis of population neural trajectories, spike trains were discretized in non-overlapping bins of 150 ms and convolved with a Gaussian kernel (width: 150 ms). Trial-averaged population activity vectors representing the instantaneous state of the system $\vec{x}_t = [x_1(t), x_2(t), \ldots, x_N(t)]$, (N is the number of units), were then projected onto the first two principal components using PCA. As previously described[59], neurons with FR < 0.5Hz were removed from this analysis (<15% of units).

To evaluate population noise levels, we calculated the average fluctuations of population activity vectors during ongoing (baseline) activity before stimulus presentations:

$$noise(\vec{X}) = \frac{1}{T}\sum_{t=1}^{T}\sqrt{\sum_{i=1}^{N}\left(x_i(t+1) - x_i(t)\right)^2},$$

where T is the length of ongoing segment and $\vec{x}_t = [x_1(t), \ldots, x_N(t)] \in \vec{X}$ is the population activity vector at time *t*. To avoid bias due to difference in population size, we used groups of ten randomly selected units (20 groups in each mouse). Units with FR < 0.1Hz were excluded from for baseline activity analysis as some units were silent during baseline times (<3% excluded). For correlations with SDI values, all unit baseline parameters were averaged and calculated per mouse.

Single-trial decoding of stimulus identity/category

To decode stimulus identity and stimulus category, we constructed maximum likelihood classifiers using encoding models of the entire population of simultaneously recorded units. Models were trained on seven randomly selected trials out of eight experimental trials for each stimulus and tested on the 8th trial. As described earlier, the best model for each training set was used to estimate the likelihood of observing each one of the stimuli, given the population responses in the held-out test trials. For each trial, we calculated the cumulative log likelihood ratio (LLR) of each of the stimulus encoding models and the model of the clean air response over time:

$$LLR_t(s_x|\vec{r}_t) = \log\left(\frac{P(\vec{r}_t|s_x)}{P(\vec{r}_t|CA)}\right); \quad cumLLR_t = \sum_{i=1}^{t} LLR_i(s_x|\vec{r}_i).$$

The trial was then classified according to the model that gave the highest likelihood at the end of stimulus presentation, $\hat{s} = \underset{x}{\operatorname{argmax}} \sum_{t \in Test} LLR_t(s_x|\vec{r}_t)$, and decoder performance was defined as the probability of choosing each one of the possible stimuli given the presentation of a specific odor. The category-based decoder was trained and tested on a combination of trials of different stimuli from the same category (social/nonsocial). Data were chosen such that the train and the test sets of the two categories would consist of the same number of trials.

Analysis of electrophysiological unit data

Neuronal data was sorted using Plexon OfflineSorter 3.2.4 (Plexon, Dallas, TX, USA), based on principal component analysis of spike waveform and inter-spike interval (ISI). Prior to sorting, the raw signal from all simultaneously recorded channels was averaged and subtracted from each channel using a custom Matlab script, in order to remove global electrical noise artifacts. To determine unit responsivity, evoked firing rates were calculated for the 5 seconds of stimulus presentation and compared to baseline firing rates during the preceding 5 seconds of baseline recordings. Response *Z*-score was calculated across repetitions per stimulus, per unit, and |Z-score| ≥ 2 threshold was used to determine responsive units and response specificity. A range of additional thresholds were also tested to provide further validation for the consistency of our results (See Extended Data Fig. 2e). Minimum empirical standard deviation (calculated across the entire data set for each stimulus) was used for Z-score analysis of units that were silent during baseline recordings, but responded during stimulus presentation (< 2 % of instances). Normalized response magnitude used for the unit-tuning analysis was evaluated as:

$\left|\frac{(Response\ FR - Baseline\ FR)}{(Response\ FR + Baseline\ FR)}\right|$, averaged per stimulus, across repetitions, and used in absolute values unless indicated otherwise. Firing rates and Z-scored PSTHs were calculated in 250 ms bins, averaged across repetitions per unit, and then averaged across all units responding to each specific stimulus (only units significantly increasing their firing rate in response to stimulus presentations were used for PSTH analysis). Single-unit firing rates were collected and averaged across 60 s of baseline recordings conducted before the initiation of experimental procedure. Due to habituation in unit responses, the first 5 presentations of each stimulus (out of 8 trials) were used for the unit analysis.

Statistical analysis

Details of specific statistical designs and appropriate tests are described for each analysis in the appropriate figure legend and throughout the text. Unless otherwise stated, data is summarized as mean ± SEM, and single data points are marked on the appropriate figures, were n denotes the number of mice for behavioral trials, the number of recording sessions for population analysis and sniffing experiments, and the number of units for single units analysis. No statistical methods were used to pre-determine sample sizes but our sample sizes were chosen based on standards in the field. If applicable, data points excluded for any reason are detailed in the appropriate Method section. Olfactory stimulus order was randomized throughout this study. Behavioral, sniffing and in-vivo electrophysiology experimental sessions were interleaved between genotypes. Experimenters were blind to mouse genotype, stimulus order and stimulus identity during experimental sessions and during initial analysis of behavioral and neural data. All statistical tests presented in this manuscript are two-tailed. Significance was set at alpha value of 0.05, and Bonferroni corrections or Dunnett's test were used when appropriate to correct for post hoc and multiple comparisons. Specific P values are detailed for each analysis in the corresponding figure legend, and in Supplementary Table 2, and significant comparisons are marked on the relevant figure panels. Levene's test was used to assess equality of variances, and statistical parameters were adjusted accordingly when needed. When applicable, data distribution was assumed to be normal but this was not formally tested. All analyses and subsequent statistical tests were performed using Matlab v2017a/b (The Mathworks Inc.), Statistica v12 software (StatSoft Inc.) and SPSS v21 (IBM Corp.). See Life Sciences Reporting Summary for additional details of statistical analysis and experimental designs.

Data availability

The data that support the findings of this study are available from the corresponding author upon reasonable request.

Code availability

The custom written analysis codes are available from the corresponding author upon reasonable request.

References

51. Franklin, K. B. J. & Paxinos, G. The Mouse Brain in Stereotaxic Coordinates 3rd ed. (Academic Press, 2008).
52. Ellegood, J. & Crawley, J. N. Behavioral and neuroanatomical phenotypes in mouse models of autism. Neurotherapeutics **12**, 521‑533 (2015).
53. Yang, M. & Crawley, J. N. Simple behavioral assessment of mouse olfaction. Curr. Protoc. Neurosci. **Chapter 8**, Unit 8.24 (2009).
54. Parabucki, A. et al. Odor concentration change coding in the olfactory bulb. eNeuro **6**, ENEURO.0396‑18.2019 (2019).
55. Schneidman, E. Towards the design principles of neural population codes. Curr. Opin. Neurobiol. **37**, 133‑140 (2016).
56. Maoz, O. & Schneidman, E. maxent_toolbox: Maximum Entropy Toolbox for MATLAB v1.02. https://doi.org/10.5281/zenodo.191625 (2017).
57. Segev, R., Ganmor, E. & Schneidman, E. A thesaurus for a neural population code. eLife **4**, e06134 (2015).
58. Lin, J. Divergence measures based on the Shannon entropy. IEEE Trans. Inf. Theory **37**, 145‑151 (1991).
59. Yu, B. M. et al. Gaussian-process factor analysis for low-dimensional single-trial analysis of neural population activity. J. Neurophysiol. **102**, 614‑635 (2009).

Extended data figures

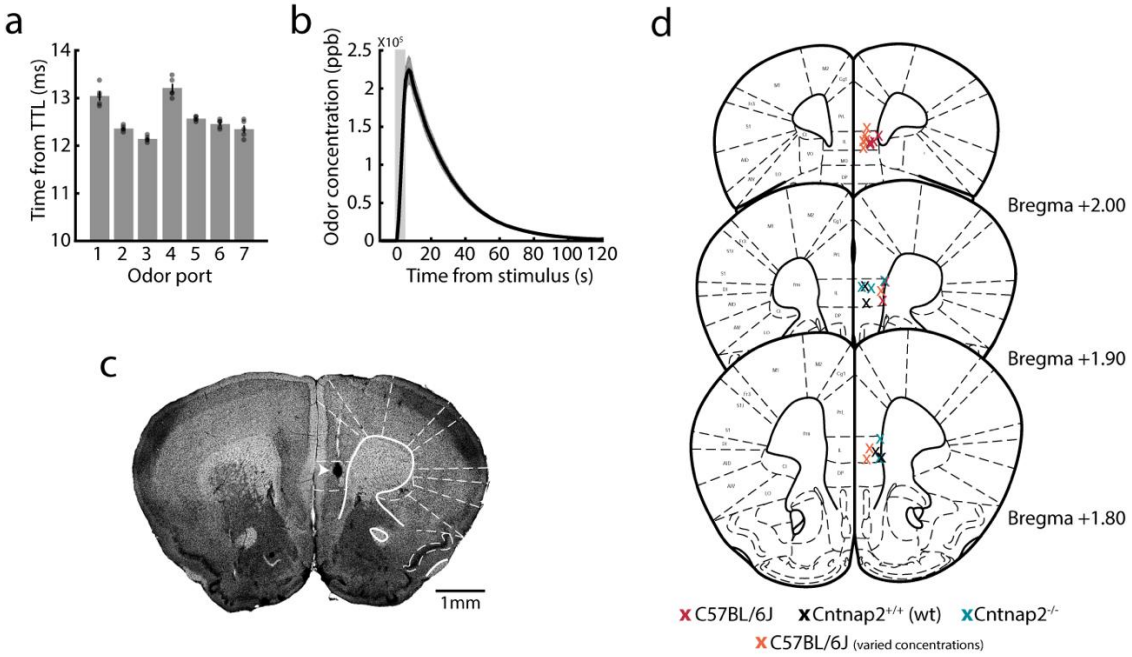

Extended Data Fig.1. Olfactometer calibrations and microarray electrode location.

(a) Latency to odor infusion from each of seven available odor ports. A pressure sensor was used to determine initiation of airflow into the chamber following TTL input indicating the opening of the appropriate solenoid. Each solenoid was tested 5 consecutive times (represented by individual circles). Mean ± s.e.m is presented. **(b)** Change in odor concentration at the center of the chamber. Measurements were taken using a volatile organic compound (VOC) meter following 5 sec infusion of vapor from a 70% ethanol solution followed by infusion of clean air (5 repetitions). Shaded area marks stimulus presentation times. Mean ± SEM is presented. **(c)** Representative image depicting the location of an electrolytic lesion used to verify electrode position in the mPFC. Arrow indicates lesion location in the infralimbic cortex. **(d)** Schematic representation of electrode placement in recorded mice from all experimental groups. Location was determined using the most ventral end of localization lesion or electrode track. Average AP coordinates are marked.

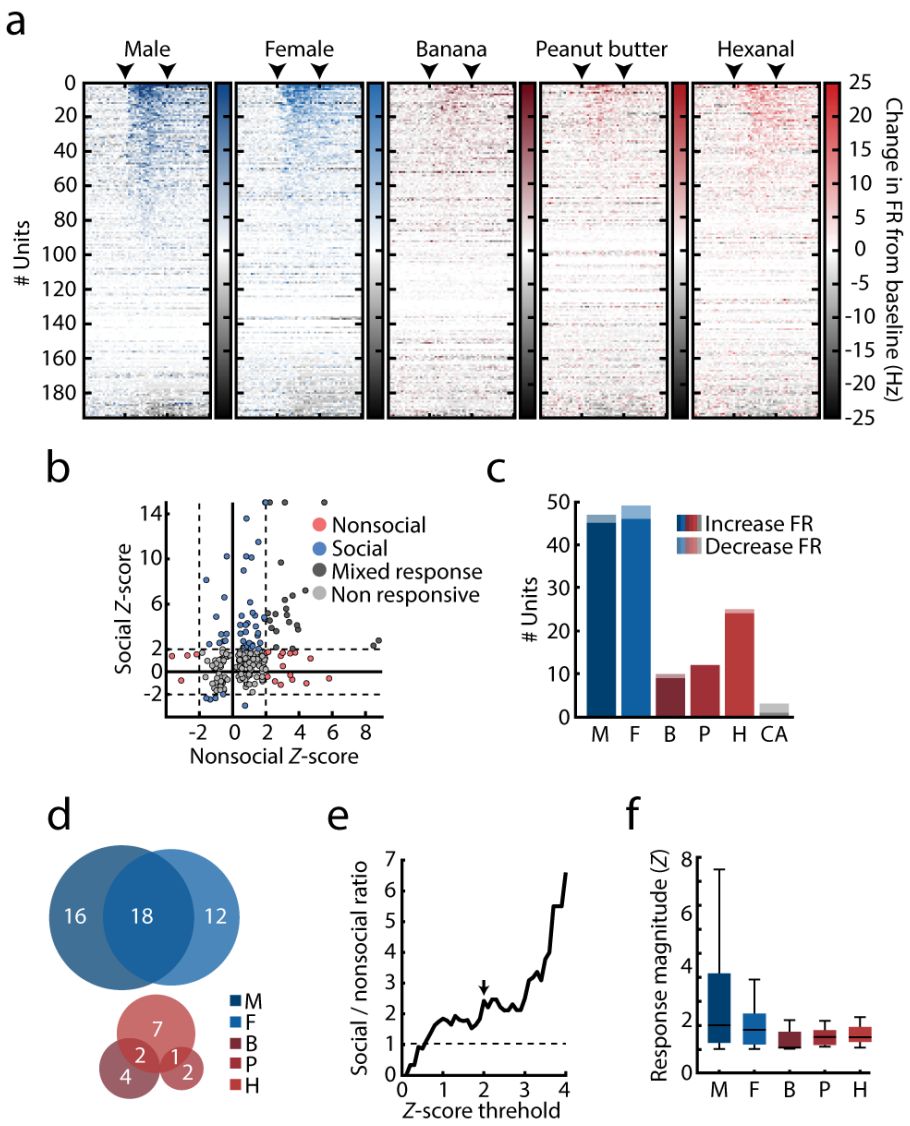

Extended Data Fig.2. Social tuning in the mPFC unit responses.

(a) Stimulus-evoked response across all recorded units per stimulus, sorted by response magnitude as calculated by the absolute change in firing rate from baseline. Color gradient represents the normalized change in firing rate calculated over 250ms bins. Arrowheads mark the time of stimulus onset and offset. **(b)** Response *Z*-score distribution calculated for all recorded units in response to social (M/F) and nonsocial (B/P/H) cues. Circles represent maximum response of individual units to each stimulus category. Color code represents response specificity. *Z* score threshold ($|Z| \geq 2$) is represented by a dashed line. Units with $Z > 15$ were assigned with $Z = 15$ for presentation purposes. **(c)** Number of units significantly increasing (dark) and decreasing (bright) their firing rates in response to each presented stimulus. Color represents stimulus identity. **(d)** Stimulus specificity overlap within social (top) and nonsocial (bottom) units. Number

of units in each category is indicated on the figure. Circle sizes are scaled to the relative number of units responding to each stimulus. **(e)** Relative ratio between social and nonsocial units, calculated using a continuous range of *Z* score thresholds. Arrow represents *Z* = 2**.** Note that the number of social units consistently exceeds that of nonsocial units starting at *Z* > 0.6 **(f)** Response magnitude for all presented stimuli for units significantly increasing their firing rate in response to stimulus presentations. Box plot depicts the interquartile range (IQR) and median, whiskers mark ±1.5*IQR. One-way ANOVA, $F_{stimulus(4,131)}$ = 1.603, *P* = 0.177. (n_M = 45 units, n_F = 46 units, n_B = 9 units, n_P = 12 units, n_H = 24 units). For all panels: M, male; F, female; B, banana; P, peanut butter; H, hexanal; CA, clean air.

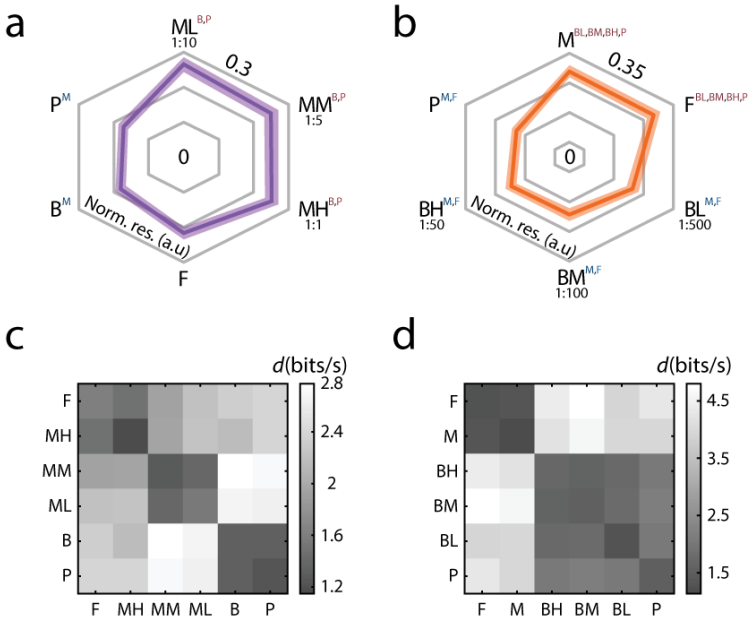

Extended Data Fig.3. Social categorization generalizes over a range of stimulus concentrations. Overall unit tuning, presented as normalized firing rate in response to male cues at three different concentrations (ML, MM, MH), female (F) banana (B) and peanut butter (P) stimuli. RM ANOVA with Bonferroni corrected post hoc comparisons. $F_{stimulus(5,440)}$ = 7.458, *P* = $9.8x10^{-7}$ (n = 89 responsive units). Superscripts mark significant post hoc comparisons. Mean ± s.e.m. (shaded area) is presented. **(b)** Overall unit tuning, presented as normalized firing rate in response to male (M) and female (F) stimuli, banana oil at three different concentrations (BL, BM, BH) and peanut butter oil (P). RM ANOVA with Bonferroni corrected post hoc comparisons. $F_{stimulus(5,285)}$ = 9.856, *P* = $1.1x10^{-8}$ (n = 58 responsive units). Superscripts mark significant post hoc comparisons. Mean ±

s.e.m (shaded area) is presented. For detailed statistics information see Supplementary Table 2. **(c)** Similarity matrices depicting the distance between population responses to the stimulus panel used in **a** (n = 4 C57BL/6J mice). **(d)** Same as c but for the stimulus panel used in **b** (n = 3 C57BL/6J mice). Norm. res.- normalized response.

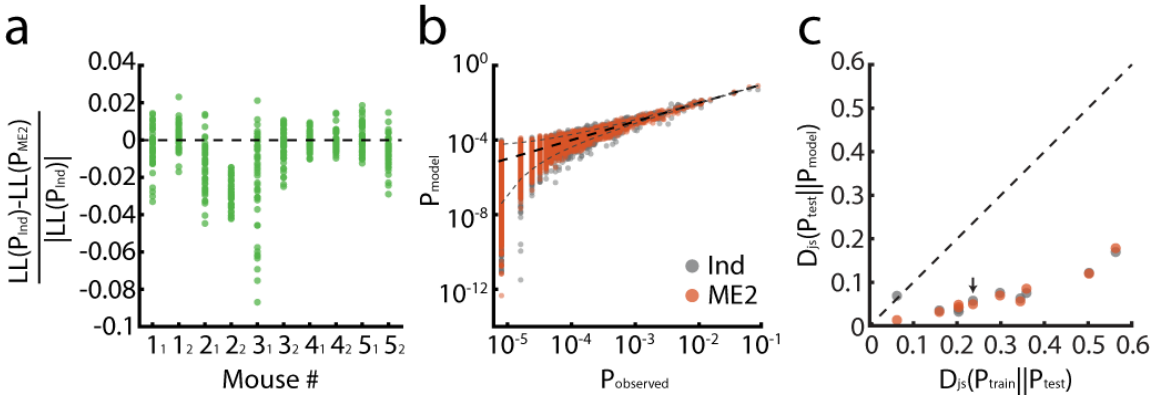

Extended Data Fig.4. Maximum entropy models accurately describe the encoding distributions of the stimuli.

(a) Normalized difference between the log-likelihood values of the pairwise maximum entropy model (ME2) and conditionally independent model, for each mouse. Models were trained over seven trials of a specific stimulus and tested on one held-out trial per stimulus. Each dot corresponds to one held-out trial for one specific stimulus (6 stimuli × 8 trials = 48 dots per mouse). Positive values indicate larger likelihood for the independent model over the ME2; the most likely model for each trial was then used for decoding analysis (see Fig. 6). **(b)** The empirical probabilities of population activity patterns of cells recorded in one mouse in response to one odor are plotted against the probabilities predicted by different models (gray dots, independent model; orange dots, ME2 model). Each dot corresponds to a single activity pattern observed during the experiment. The funnel marked by the dashed gray line indicates 99% confidence interval of the empirical measurement. Black dashed line shows equality. **(c)** The Jensen–Shannon divergences between the empirical joint probability distribution of activity patterns and the different models – ME2 (orange) and conditionally independent (gray). Black line indicates equality of the distance of the models from the test data, and the distance between the training and test data. Models were trained using randomly chosen 1750 samples, similar to the number of training data sample used for the decoding analysis (7 trials of 5 seconds each). Analysis was

done using all recorded units from each mouse (up to 20 units) and the mean over ten randomly chosen training sets is plotted. While no model is consistently better than the other in capturing the distribution across all mice, both models clearly outperform the empirical model. Arrow indicates the example mouse shown in panel **b**.

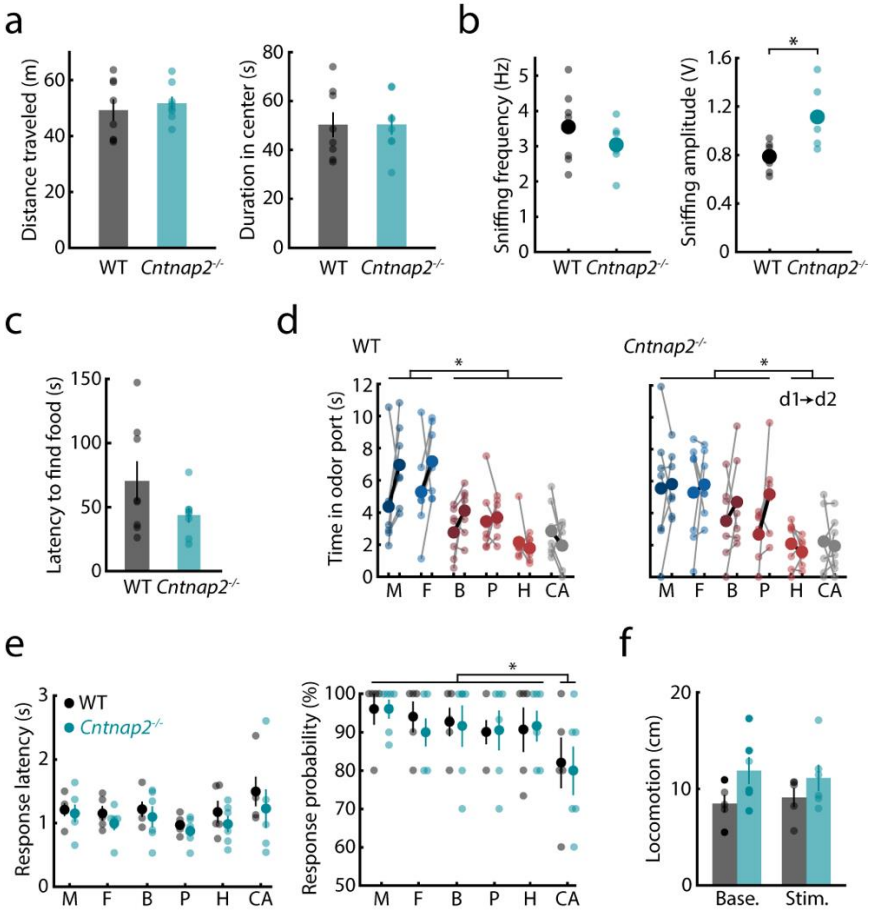

Extended Data Fig.5. Behavioral analysis of *Cntnap2*$^{-/-}$ mice.

(a) Open field test. Left*:* Mean distance travelled during test for WT (black, n = 8) and *Cntnap2*$^{-/-}$ mice (teal, n = 8). Two-sided Mann-Whitney U test, U = 28, P = 0.721. *Right*: Mean duration in center of arena. Two-sided Mann-Whitney U test, U = 28, P = 0.721. **(b)** Baseline sniffing quantifications for WT (black, n = 7 recording sessions) and *Cntnap2*$^{-/-}$ mice (teal, n = 6 sessions). Left: baseline sniffing frequency. Mann-Whitney U test, U = 26, P = 0.52. Right: baseline sniff amplitude Mann-Whitney U test, U = 4, P = 0.014. Circles represents individual recording sessions. **(c)** Mean duration to find a buried food pellet for WT (black, n = 8) and *Cntnap2*$^{-/-}$ mice (teal, n = 8). Two-sided Mann-Whitney U test, U = 20, P = 0.234. **(d)** Mean duration of odor exploration, calculated as time sniffing odor port for WT (left, n =7) and *Cntnap2*$^{-/-}$ mice (right, n = 7 mice). Duration is presented for first and second day of experiment (left to right) for each odor and each mouse. Two-way RM ANOVA with Bonferroni corrections. For WT: $F_{stimulus(5,30)}$ = 15.444, P = 1.6x10^{-7}; $F_{day(1,6)}$ = 2.756, P = 0.148; $F_{stimulus*day(5,30)}$ = 1.777, P = 0.148; for *Cntnap2*$^{-/-}$: $F_{stimulus(5,30)}$ = 11.862, P = 2.2x10^{-8}; $F_{day(1,6)}$ = 0.593, P = 0.470; $F_{stimulus*day(5,30)}$ = 1.777, P = 0.203; **(e)** Left: Average latency to

odor-evoked orientation responses for WT (black, n = 5) and *Cntnap2*$^{-/-}$ (teal, n = 6) mice in odor infusion chamber. Circles represent individual mice. Mixed-design RM ANOVA. $F_{genotype(1,9)} = 0.959$, $P = 0.352$; $F_{stimulus(5,45)} = 2.449$, $P = 0.048$ with Dunnett's test against clean air; $F_{genotype*stimulus(5,45)} = 0.163$, $P = 0.974$. Right: mean probability of odor-evoked orientation responses. Mixed-design RM ANOVA. $F_{genotype(1,9)} = 0.040$, $P = 0.844$; $F_{stimulus(5,45)} = 3.304$, $P = 0.013$ with Dunnett's test against clean air; $F_{genotype*stimulus(5,45)} = 0.115$, $P = 0.988$ **(f)** Locomotion levels of WT (black, n = 5) and *Cntnap2*$^{-/-}$ mice (teal, n = 6) in the odor infusion chamber during baseline and stimulus presentation (averaged across all presented odors). Two-sided Mann-Whitney U Test, For baseline: $U = 7$, $P = 0.171$; For stimulus: $U = 10$, $P = 0.411$. Circles represent individual mice unless otherwise indicated. For all panels: Mean ± s.e.m. is presented. Note that some individual data points and error bars are covered by the mark of the mean. *$P < 0.05$. For detailed statistics information see Supplementary Table 2. M, male; F, female; B, banana; P, peanut butter; H, hexanal; CA, clean air. Base., baseline; Stim., Stimulus.

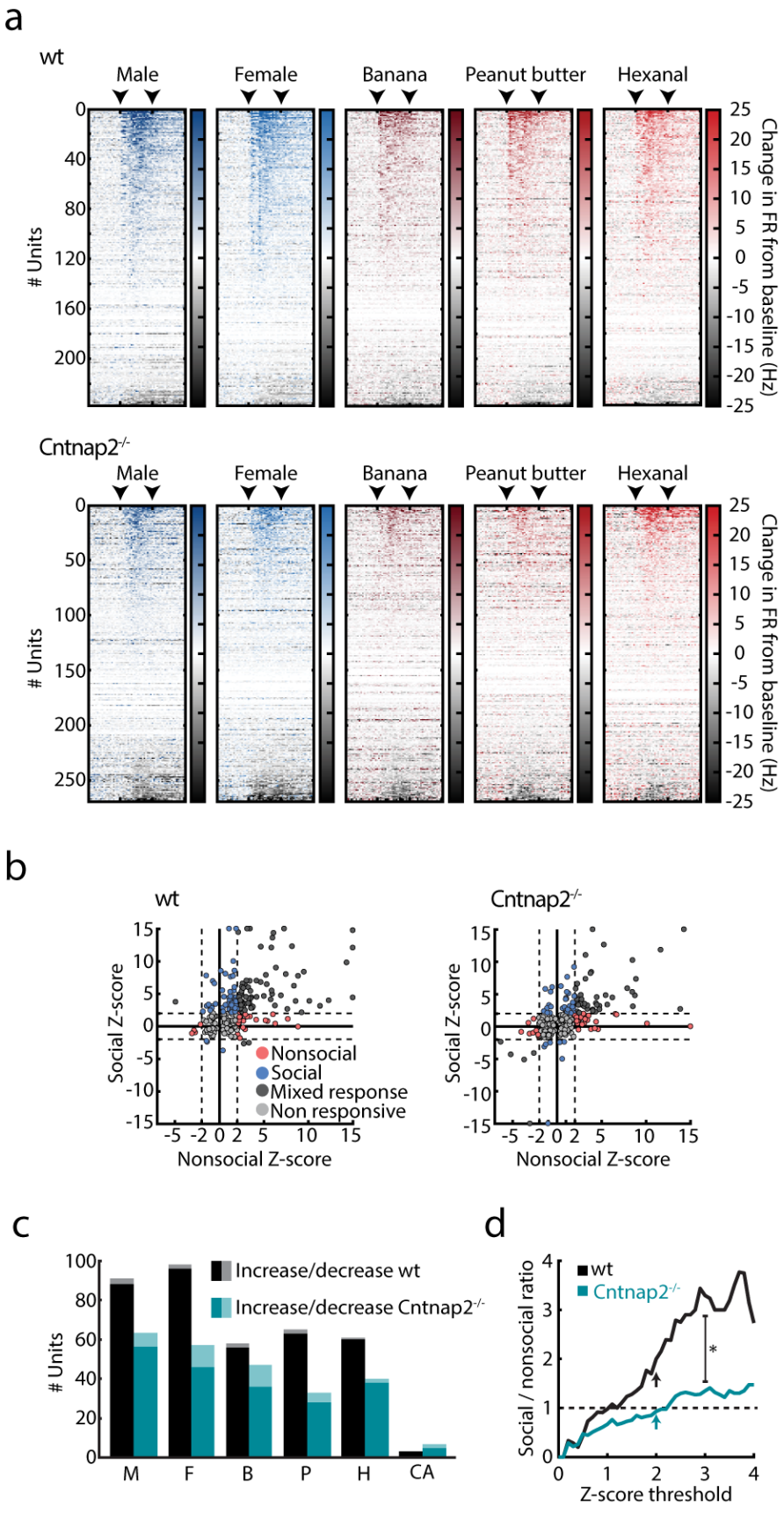
a
wt
Male
Female
Banana
Peanut butter
Hexanal
Units
Change in FR from baseline (Hz)
Cntnap2-/-
b
wt
Cntnap2-/-
Social Z-score
Nonsocial Z-score
Nonsocial
Social
Mixed response
Non responsive
c
Increase/decrease wt
Increase/decrease Cntnap2-/-
Units
M
F
B
P
H
CA
d
wt
Cntnap2-/-
Social / nonsocial ratio
Z-score threshold

Extended Data Fig.6. Altered response patterns to social and nonsocial stimuli in the mPFC of *Cntnap2*$^{-/-}$ mice.

(a) Stimulus-evoked responses across all recorded units per stimulus, sorted by response magnitude as calculated by the change in firing rate from baseline for WT (top) and *Cntnap2*$^{-/-}$ (bottom) mice. Color gradient represents the change in firing rate from baseline, calculated over 250ms bins. Arrows mark the time of stimulus onset and offset. **(b)** Response *Z*-score distribution calculated for all recorded units in WT (left) and *Cntnap2*$^{-/-}$ mice (right) in response to social (M/F) and nonsocial (B/P/H) cues. Circles represent maximum response of individual units to each stimulus category. Color code represents response specificity. Z score threshold ($|Z| \geq 2$) is represented by a dashed line. Units with $Z > 15$ were assigned with $Z = 15$ for presentation purposes. **(c)** Number of units significantly increasing (dark) and decreasing (bright) their firing rates in response to each presented stimulus in WT (black) and *Cntnap2*$^{-/-}$ (teal) mice. **(d)** Relative ratio between social and nonsocial units, calculated using a continuous range of Z score thresholds for WT (black) and *Cntnap2*$^{-/-}$ (teal) mice. Arrows represent $Z = 2$**.** Linear regression analysis ($0 \leq Z \leq 3$, n = 32 measurements for each genotype), $F_{WT(1,30)} = 1088.42$, $P = 3.9X10^{-25}$, $R^2_{WT} = 0.973$. $F_{Cntnap2-/-(1,30)} = 652.294$, $P = 6.5X10^{-22}$, $R^2_{Cntnap2-/-} = 0.956$. $B_{WT} = 1.106$, $B_{Cntnap2-/-} = 0.425$, with non-overlapping 95% confidence intervals as a measure of statistical significant difference between regression lines. For all panels: *P < 0.05, M, male; F, female; B, banana; P, peanut butter; H, hexanal; CA, clean air.

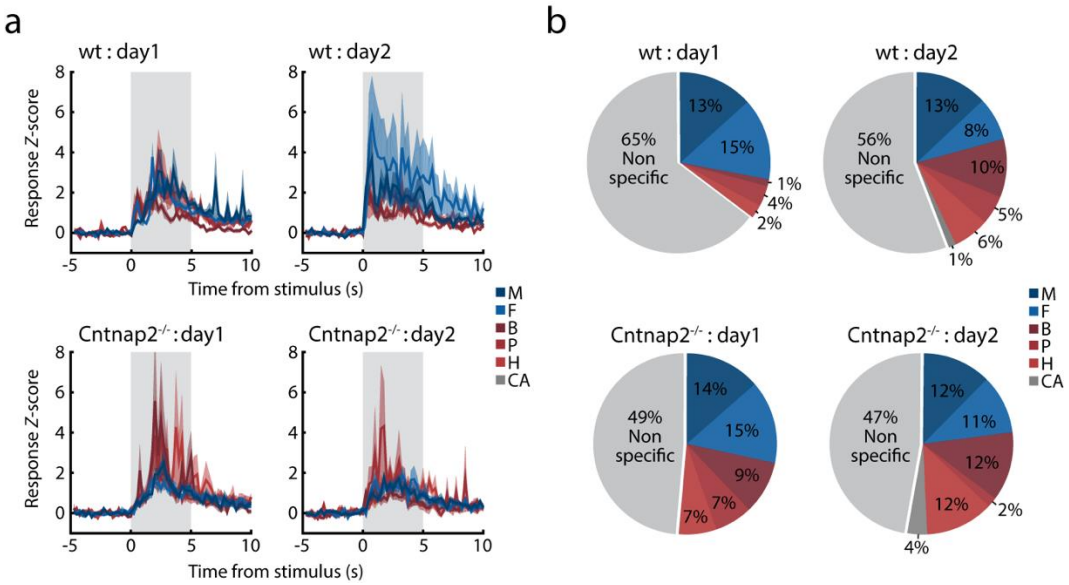

Extended Data Fig.7. Experience-dependent changes in stimulus-evoked unit responses.

(a) Stimulus-evoked PSTHs portraying mean response *Z*-score of cue-responsive units in the first (left) and second (right) recording sessions, for WT (top) and *Cntnap2*$^{-/-}$ (bottom) mice. Color code represent stimulus identity. Shaded areas mark stimulus presentation time. Mean ± s.e.m. is presented. **(b)** Stimulus specificity among cue responsive units in the first (left) and second (right) recording sessions, in WT (top) and *Cntnap2*$^{-/-}$ (bottom) mice. Colors represent stimulus identity. For WT, n_{day1} = 82 units, n_{day2} = 77 units; for *Cntnap2*$^{-/-}$ mice, n_{day1} = 74 units, n_{day2} = 57 units. For all panels: M, male; F, female; B, banana; P, peanut butter; H, hexanal; CA, clean air.

Supplementary information

Supplementary Table 1. Unit stimulus-evoked response magnitude is not correlated with stimulus-evoked change in behavioral locomotion. Response Z-score values were calculated for all units responding to each odor in each mouse in each recording session (in absolute values, averaged over all responsive units, per odor per session. n_{WT} = 10 sessions, $n_{Cntnap2-/-}$ = 11 sessions). Pearson's correlations were then used to assess correlation of unit response magnitude with the corresponding change in behavioral locomotion during infusion of odor stimuli compared to baseline.

	Male	Female	Banana	Peanut butter	Hexanal
Wild-type	r = 0.162 P = 0.654 $t_{(8)}$ = 0.466	r = 0.178 P = 0.623 $t_{(8)}$ = 0.512	r = 0.071 P = 0.846 $t_{(8)}$ = 0.2	r = -0.122 P = 0.737 $t_{(8)}$ = -0.347	r = 0.307 P = 0.389 $t_{(8)}$ = 0.912
***Cntnap2*$^{-/-}$**	r = -0.321 P = 0.335 $t_{(9)}$ = -1.018	r = 0.015 P = 0.964 $t_{(9)}$ = 0.046	r = -0.228 P = 0.5 $t_{(9)}$ = -0.703	r = 0.013 P = 0.970 $t_{(9)}$ = 0.038	r = 0.420 P = 0.199 $t_{(9)}$ = 1.387

Supplementary Table 2. Comprehensive statistical information of all post-hoc comparisons presented in this publication.

Figure	Test	Comparison	P-value
Fig. 1c	Two-sided Wilcoxon signed-ranked	Social & Nonsocial	0.028
		Social & Clean air	0.028
		Nonsocial & Social	0.028
		Nonsocial & Clean air	0.028
		Clean air & Social	0.028
		Clean air & Nonsocial	0.028
Fig. 2e	Bonferroni corrected post-hoc comparisons (following RM ANOVA)	M & F	1.000
		M & B	$1.6x10^{-10}$
		M & P	$8.1x10^{-12}$
		M & H	$7.1x10^{-7}$
		F & B	$1.8x10^{-10}$
		F & P	$9.8x10^{-12}$
		F & H	$7.8x10^{-7}$
		B & P	1.000
		B & H	1.000
		P & H	0.539
Fig. 3d	Bonferroni corrected post-hoc comparisons (following RM ANOVA)	M & F	1.000
		M & B	$3.7x10^{-6}$
		M & P	$3.9x10^{-5}$
		M & H	$2.5x10^{-5}$
		F & B	$9.3x10^{-5}$
		F & P	$9x10^{-4}$
		F & H	$5.9x10^{-4}$
		B & P	1.000
		B & H	1.000
		P & H	1.000
Fig. 3e	Dunnet's post hoc comparisons against last baseline bin (following 2-way RM ANOVA)	M & F sec 1	0.019
		M & F sec 2	0.006
		M & F sec 3	0.007
		M & F sec 4	0.034
		M & F sec 5	0.807
		M & F sec 6	0.738

		M & Nonsocial sec 1	0.530
		M & Nonsocial sec 2	2.05×10^{-5}
		M & Nonsocial sec 3	2.05×10^{-5}
		M & Nonsocial sec 4	2.06×10^{-5}
		M & Nonsocial sec 5	2.44×10^{-5}
		M & Nonsocial sec 6	2.6×10^{-4}
		M & Nonsocial sec 7	0.006
		M & Nonsocial sec 8	0.006
		M & Nonsocial sec 9	0.018
		M & Nonsocial sec 10	0.015
		M & Nonsocial sec 11	0.069
Fig 4a	Bonferroni corrected post-hoc comparisons (following mixed-design RM ANOVA)	WT: Social & Object	0.022
		Cntnap2$^{-/-}$: Social & Object	0.760
Fig 4b	Bonferroni corrected post-hoc comparisons (following mixed-design RM ANOVA)	WT: Social 1 & Social 2	0.008
		Cntnap2$^{-/-}$: Social 1 & Social 2	0.761
Fig 4d	Bonferroni corrected post-hoc comparisons (following RM ANOVA)	WT: M & F	1.000
		WT: M & B	0.049
		WT: M & P	0.013
		WT: M & H	3.4×10^{-5}
		WT: M & CA	5.7×10^{-5}
		WT: F & B	0.026
		WT: F & P	0.007
		WT: F & H	1.8×10^{-5}
		WT: F & CA	2.9×10^{-5}
		WT: B & P	1.000
		WT: B & H	0.203
		WT: B & CA	0.310
		WT: P & H	0.619
		WT: P & CA	0.905

		WT: H & CA	1.000
	Bonferroni corrected post-hoc comparisons (following RM ANOVA)	*Cntnap2*$^{-/-}$: M & F	1.000
		Cntnap2$^{-/-}$: M & B	1.000
		Cntnap2$^{-/-}$: M & P	1.000
		Cntnap2$^{-/-}$: M & H	0.004
		Cntnap2$^{-/-}$: M & CA	0.011
		Cntnap2$^{-/-}$: F & B	1.000
		Cntnap2$^{-/-}$: F & P	1.000
		Cntnap2$^{-/-}$: F & H	0.005
		Cntnap2$^{-/-}$: F & CA	0.012
		Cntnap2$^{-/-}$: B & P	1.000
		Cntnap2$^{-/-}$: B & H	0.078
		Cntnap2$^{-/-}$: B & CA	0.184
		Cntnap2$^{-/-}$: P & H	0.023
		Cntnap2$^{-/-}$: P & CA	0.058
		Cntnap2$^{-/-}$: H & CA	1.000
Fig 4f	Bonferroni corrected post-hoc comparisons (following mixed-design RM ANOVA)	M & F	1.000
		M & B	0.395
		M & P	0.021
		M & H	0.104
		M & CA	4.5×10^{-9}
		F & B	0.603
		F & P	0.037
		F & H	0.169
		F & CA	9×10^{-9}
		B & P	1.000
		B & H	1.000
		B & CA	2.3×10^{-5}
		P & H	1.000
		P & CA	0.001
		H & CA	1.5×10^{-4}
Fig 4g	Bonferroni corrected post-hoc comparisons (following mixed-design RM ANOVA)	M & F	1.000
		M & B	0.012
		M & P	0.263
		M & H	2×10^{-4}
		M & CA	8.7×10^{-7}
		F & B	0.021
		F & P	0.412

		F & H	$3.7x10^{-4}$
		F & CA	$1.7x10^{-6}$
		B & P	1.000
		B & H	1.000
		B & CA	0.131
		P & H	0.343
		P & CA	0.005
		H & CA	1.000
Fig. 5b	Bonferroni corrected post-hoc comparisons (following RM ANOVA for stimulus effect in WT. F = 13.387, P = $1.7x10^{-10}$)	WT: M & F	1.000
		WT: M & B	$7.8x10^{-7}$
		WT: M & P	$2.4x10^{-5}$
		WT: M & H	0.007
		WT: F & B	$7.9x10^{-7}$
		WT: F & P	$2.5x10^{-5}$
		WT: F & H	0.007
		WT: B & P	1.000
		WT: B & H	0.430
		WT: P & H	1.000
	Bonferroni corrected post-hoc comparisons (following RM ANOVA for stimulus effect in *Cntnap2*$^{-/-}$: F = 3.332, P = 0.01)	*Cntnap2*$^{-/-}$: M & F	1.000
		Cntnap2$^{-/-}$: M & B	0.140
		Cntnap2$^{-/-}$: M & P	0.093
		Cntnap2$^{-/-}$: M & H	0.040
		Cntnap2$^{-/-}$: F & B	0.824
		Cntnap2$^{-/-}$: F & P	0.602
		Cntnap2$^{-/-}$: F & H	0.309
		Cntnap2$^{-/-}$: B & P	1.000
		Cntnap2$^{-/-}$: B & H	1.000
		Cntnap2$^{-/-}$: P & H	1.000
Fig. 5e	Bonferroni corrected post-hoc comparisons (following mixed-design RM ANOVA)	WT: day 1 & day 2	0.002
		Cntnap2$^{-/-}$: day1 & day 2	1.000
Fig. 5f	Bonferroni corrected post-hoc comparisons (following 2-way RM ANOVA)	WT: S;S day 1 & S;S day 2	0.031
		WT: NS;NS day 1 & NS;NS day 2	0.062
		WT: S;NS day 1 & S;NS day 2	0.042
Extended Data Fig.3a	Bonferroni corrected post-hoc comparisons (following RM ANOVA)	ML & MM	1.000
		ML & MH	1.000
		ML & F	0.292

		ML & B	0.001
		ML & P	$1.2x10^{-4}$
		MM & MH	1.000
		MM & F	1.000
		MM & B	0.010
		MM & P	0.002
		MH & F	1.000
		MH & B	0.007
		MH & P	0.002
		F & B	1.000
		F & P	0.453
		B & P	1.000
Extended Data Fig.3b	Bonferroni corrected post-hoc comparisons (following RM ANOVA)	BL & BM	1.000
		BL & MH	1.000
		BL & P	1.000
		BL & M	0.009
		BL & F	0.017
		BM & BH	1.000
		BM & P	1.000
		BM & M	$2.7x10^{-4}$
		BM & F	0.001
		BH & P	1.000
		BH & M	0.001
		BH & F	0.001
		P & M	$1.1x10^{-5}$
		P & F	$2.7x10^{-5}$
		M & F	1.000
Extended Data Fig.5d	Bonferroni corrected post-hoc comparisons (following 2-way RM ANOVA)	WT: M & F	1.000
		WT: M & B	0.018
		WT: M & P	0.031
		WT: M & H	$2.4x10^{-5}$
		WT: M & CA	$1.6x10^{-4}$
		WT: F & B	0.001
		WT: F & P	0.003
		WT: F & H	$1.9x10^{-6}$
		WT: F & CA	$1.3x10^{-5}$
		WT: B & P	1.000
		WT: B & H	0.364
		WT: B & CA	1.000
		WT: P & H	0.225

		WT: P & CA	1.000
		WT: H & CA	1.000
	Bonferroni corrected post-hoc comparisons (following 2-way RM ANOVA)	*Cntnap2*$^{-/-}$: M & F	1.000
		Cntnap2$^{-/-}$: M & B	0.390
		Cntnap2$^{-/-}$: M & P	0.209
		Cntnap2$^{-/-}$: M & H	4.6×10^{-5}
		Cntnap2$^{-/-}$: M & CA	1.3×10^{-4}
		Cntnap2$^{-/-}$: F & B	0.629
		Cntnap2$^{-/-}$: F & P	0.347
		Cntnap2$^{-/-}$: F & H	8.5×10^{-5}
		Cntnap2$^{-/-}$: F & CA	2.4×10^{-4}
		Cntnap2$^{-/-}$: B & P	1.000
		Cntnap2$^{-/-}$: B & H	0.031
		Cntnap2$^{-/-}$: B & CA	0.081
		Cntnap2$^{-/-}$: P & H	0.062
		Cntnap2$^{-/-}$: P & CA	0.158
		Cntnap2$^{-/-}$: H & CA	1.000
Extended Data Fig.5e	Dunnett's test against clean air (following mixed-design RM ANOVA).	Latency: M	0.288
		Latency: F	0.066
		Latency: B	0.213
		Latency: P	0.004
		Latency: H	0.072
		Probability: M	0.001
		Probability: F	0.016
		Probability: B	0.013
		Probability: P	0.039
		Probability: H	0.023